# MESH-CTEM – DEVELOPMENT AND TESTING OF AN INTEGRATED BIOGEOCHEMICAL AND WATERSHED HYDROLOGICAL MODELLING SYSTEM

**By Stéfan Joseph Sauer, B.Sc.**

**A Thesis Submitted to the School of Graduate Studies in Partial Fulfillment of the Requirements for the Degree Master of Science**

**MASTER OF SCIENCE (2019)** **MCMASTER UNIVERSITY**
**(EARTH AND ENVIRONMENTAL SCIENCE)** **HAMILTON, ONTARIO**

TITLE: MESH-CTEM – DEVELOPMENT AND TESTING OF AN THE INTEGRATED BIOGEOCHEMICAL AND WATERSHED HYDROLOGICAL MODELLING SYSTEM
AUTHOR: Stéfan Joseph Sauer

SUPERVISOR: Dr. M. A. Arain

NUMBER OF PAGES: 56,

# Abstract

This study developed an integrated biogeochemical and hydrological modelling system by incorporating the latest versions of the nitrogen coupled Canadian Land Surface Scheme-Canadian Terrestrial Ecosystem Model (CLASS-CTEM) into the Modélisation Environmentale Communautaire (MEC) Surface and Hydrology system (MESH), hereafter referred to as MESH-CTEM. The newly developed MESH-CTEM modelling system allows simulations of energy, water, carbon and nitrogen fluxes and their feedbacks on vegetation growth and exploration of impacts of future climatic changes on catchment-scale processes. Performance of the MESH-CTEM system was tested at the Big Creek watershed within Norfolk county, Ontario, Canada, which is a 573 $km^2$ crop-dominated catchment with areas of broadleaf and needleleaf forests, using observed eddy covariance flux, meteorological and hydrological datasets from October 2004 to December 2017 at a grid resolution of $0.02^o$ latitude × $0.02^o$ longitude. MESH-CTEM showed a significant increase in the simulated streamflow as compared to MESH running with only CLASS, excluding dynamic vegetation growth and carbon fluxes, resulting in an overall increase in the accuracy of streamflow with Nash-Sutcliffe Efficiency (NSE) indices of 0.38 and 0.12 respectively. Significant improvements were also seen for each Plant Functional Type (PFT) within the catchment with respect to energy fluxes, evaporation and soil water regimes. Many of these improvements in simulated fluxes were due in part by changes in the canopy conductance formulation, more realistic soil heat and water processes due to the introduction of fine soil layers, inter-grid transfers of water and other spatial components and vegetation cover feedbacks on energy, water and carbon exchanges by using dynamic vegetation growth processes. Simulated averaged gross ecosystem productivity, ecosystem respiration, latent heat flux and sensible heat flux for the entire catchment were respectively 660 g C $m^{-2}$ $yr^{-1}$, 640 g C $m^{-2}$ $yr^{-1}$, 32.5 W $m^{-2}$ and 27.1 W $m^{-2}$. Application and use of MESH-CTEM will help to study the impact of climate change and extreme events on energy, water and carbon fluxes

and associated feedbacks at the catchment scale. Additionally, this will help bridge a major gap in hydrologic modelling studies through integration of biogeochemical processes.

# Acknowledgements

I would like to thank several people who helped put this project together.

First of all, I would like to thank my supervisor for my master's thesis and undergraduate thesis, Dr. Altaf Arain. I will be forever grateful that you accepted me as your undergraduate thesis student all those years ago. My thanks as well to Dr. Sang-Tae Kim, Dr. Sean Carey and Dr. Paulin Coulibaly for agreeing to review my thesis and to be part of my defense committee. For helping me understand the ins and outs of the CLASS-CTEM and MESH models and for dealing with my flow of e-mails, I would like to thank Daniel Princz, Dr. Paul Bartlett, Dr. Bruce Davison, Dr. Joe Melton, Dr. Vivek Arora and many other researchers of the Global Water Futures (GWF) program. My sincere thanks to Dr. Suo Huang and Ben Windeler, although our encounters have been brief, this thesis and current model could not have been accomplished without your extensive work on providing a functioning and understandable CLASS-CTEM-N+ model.

I would like also thank the climate lab and all of the things that we've accomplished, including the AFL league, following Ligue 2 matches, those darn litter traps and dealing with my obviously funny sense of humour. It's been my pleasure to work with you all for these years: Eric Beamesderfer, Alanna Bodo, Brandon Burns, Olivier Champagne, Shawn McKenzie, Tariq Deen, David Ma, Rizwan Mohammed, You Ghangyong, Keegan Smith and Ian Martin. Thanks as well to Katherine Philp, Dr. Jason Brodeur and Dr. Myroslava Khomik for your ongoing help for the lab and the McMaster Centre for Climate Change.

Some unsung people who have surely helped me become the person I am today have been many of my instructors at McMaster during my undergraduate education. Many thanks to the Mathematics &

Statistics department for teaching me a variety of mathematical skills and for providing me with a hard earned minor in Mathematics, something I never could have imagined as a kid. I would also like to thank the Physics & Astronomy department for inspiring me to continue pursuing a degree in science and for teaching me that nothing worth knowing can be taught. My thanks to Patrick DeLuca and the GIS faculty at McMaster for teaching me fundamental and advanced skills in GIS, which is something that will surely help me as I search for a career. My thanks to everyone else in the School of Geography and Earth Sciences for helping me in completing my degrees after all these years.

Finally, I could not end these acknowledgements without mentioning my family. To the Sauer family, thank you very much for your support over all these years with my time as a student.

A special thanks to my life partner Josée Ménard with her love and support for these past 3 years, especially helping me with everything from becoming more independent to learning how to toast bread over an open fire.

# Symbols and Abbreviations

| | |
|---|---|
| $A_n$ | Canopy Photosynthesis Rate |
| BDC | Broadleaf |
| BDL-DCD-COLD | Broadleaf-Deciduous-Cold |
| BDL-DCD-DRY | Broadleaf Deciduous Dry |
| BDL-EVG | Broadleaf Evergreen |
| CanESM | Canadian Earth System Model |
| CaPA | Canadian Precipitation Analysis |
| CLASS | Canadian Land Surface Scheme |
| cm | Centimeter |
| CMIP5 | Climate Modelling Intercomparison Project |
| CTEM | Canadian Terrestrial Ecosystem Model |
| $CO_2$ | Carbon Dioxide |
| CR | Crops |
| $D$ | Vapour Pressure Deficit |
| $D_D$ | Drainage Density |
| $d_e$ | Depth above ponded water |
| DDS | Dynamically Dimensioned Search |
| DEM | Digital Elevation Model |
| ECCC | Environment and Climate Change Canada |
| ESM | Earth System Model |
| ET | Evapotranspiration |
| g C | Grams of Carbon |
| GEP | Gross Ecosystem Productivity |
| GR | Grasses |
| GRU | Grouped Response Unit |

| | |
|---|---|
| GWF | Global Water Futures |
| Kg | Kilogram |
| $K_{S0}$ | Horizontal Saturated hydraulic conductivity |
| LAI | Leaf Area Index |
| *m* | Meter |
| MAE | Mean Absolute Error |
| MEC | Modélisation Environnementale Communautaire |
| mm | Millimeter |
| *n* | Sample Size |
| NDL-EVG | Needleleaf – Evergreen |
| NDL-DCD | Needleleaf – Decidous |
| NEP | Net Ecosystem Productivity |
| NL | Needleleaf |
| NRCan | Natural Resources Canada |
| NSE | Nash-Sutcliffe Efficientcy |
| PFT | Plant Functional Type |
| $q_{\text{Base}}$ | Baseflow |
| $q_{\text{Int}}$ | Interflow |
| $q_{\text{over}}$ | Overland Flow Runoff |
| $r_c$ | Canopy Resistance |
| Re | Ecosystem Respiration |
| RDPS | Regional Deterministic Prediction Model |
| Rn | Net Radiation |
| *s* | Second |
| TP39 | Turkey Point 1939 |
| TPD | Turkey Point Deciduous |

| | |
|---|---|
| ULM | Unified Modelling Language |
| VWC | Volumetric Water content |
| $W$ | Watt |
| WATFLOOD | Waterloo Flood Forecasting Model |
| $\alpha$ | Albedo |
| $\Theta_S$ | Volumetric Water content at Saturation |
| $\Lambda$ | Slope Percentage |
| $\Gamma$ | Carbon Dioxide compensation point |

# Table of Contents

# List of Tables

# List of Figures

## 1. Introduction

Hydrological models play an important role in water resources management due to their capabilities to simulate, visualize and help understand the hydrological cycle and its numerous associated complex processes. These models simulate multiple hydrological processes on a variety of spatial and temporal scales (Singh and Frevert, 2002). Modelling these watershed-scale processes is considered important for the forecasting of flooding events, water resource management, soil erosion, nutrient circulation and water quality (Santhi et al., 2006; Devia et al., 2015). To provide more accurate quantitative responses of watershed-scale processes, these models have been under constant development. Some recent examples of advancements include implementation of multi-dimensional flow equations (Dargahi and Setegn, 2011), more intricate methods of watershed delineation (O'Callaghan and Mark, 1984; Jones et al., 1990) and higher spatial resolution (Kornelsen et al., 2016; Chen et al., 2017). Furthermore, numerous studies have emphasized the importance of advancing development of watershed-scale hydrological models (Arnold and Fohrer, 2005; McDonnell et al., 2007; Daniel, 2011; Davison et al., 2016). In particular, to address the uncertainties in hydrological processes caused by the changes in regional water regimes due to climate change and extreme weather events (Xu and Singh, 2004; Chen et al., 2011). These improvements will undoubtedly continue to provide a greater understanding of hydrological processes and aid in the development of more representative simulations of watersheds in changing environments.

With respect to the development of watershed models, one of the most significant problems is the limitation or lack of processes being represented (Fatichi et al., 2016). More specifically, hydrological models have traditionally focused on simulations within the hydrological realm rather than the direct or indirect impacts and relationships with other environmental processes (Singh and Frevert, 2002; McDonnell et al., 2007). These processes range from small-scale anthropogenic disruption (Leavesley et al., 1983; Arnold et al., 1993), to the long-term effect of sediment transport from stream channels (Wicks and Bathurst, 1996; Heppner et al., 2006) and the incorporation of land-surface atmosphere interactions such as radiative exchanges, evapotranspiration and dynamic weather patterns (Pan and Mahrt, 1987; Verseghy, 1991). Land-surface atmosphere interactions have become ubiquitous within the modern process-based watershed-scale hydrological models (Verseghy, 1991; Liang et al., 1994; Pietroniro et al.,

2007; Lawrence et al., 2011).

Despite these recent developments, modern process-based hydrological models still have significant limitations because of the absence of a number of important processes, including the complex interactions with the vegetation ecology and biogeochemical processes (Janauer, 2000; Rodriguez-Iturbe, 2000; Bond, 2003; Thornton et al., 2009). Examples of these processes include stomatal control on evapotranspiration (ET) (Monteith, 1965). Additionally, there are also feedbacks on hydrological processes from biota, such as the ability of flora to influence infiltration, surface and sub-surface runoff (Troendle and King, 1987; Betoldi et al., 2014). These interactions and associated feedbacks can take place on a variety of spatial and temporal scales (Janauer, 2000; Porporato and Rodriguez-Iturbe., 2002; Zalewski, 2002; Tetzlaff et al., 2007). The importance of ecological and hydrological interactions have been recognized by the climate modelling community (Clark et al., 2015a). The most recent phase of the Climate Modelling Intercomparison Project (CMIP5) has also recognized and emphasized the importance of integrating biogeochemical cycling and hydrological processes into Earth System Models (ESMs) (Taylor et al., 2012). Furthermore, several terrestrial ecosystem models have been developed, which emphasize ecological and hydrological interactions and feedbacks on a variety of temporal and spatial scales (Arora and Boer, 2003; Gerten et al., 2004; Tague and Band, 2004; Krysanova and Arnold, 2008). At the same time, ecological and biogeochemical cycling algorithms have also been introduced into recent watershed-scale hydrological models (Lawrence et al., 2011; Chen et al, 2015). Even with these recent developments, there are still significant limitations in the modelling of coupled biogeochemical and hydrological processes, in particular at catchment scales.

The goal of this research is to develop an integrated biogeochemical and hydrologic modelling system that can be applied at a catchment scale for water resources and carbon fluxes studies. For this purpose, the Canadian Land Surface Scheme and Canadian Terrestrial Ecosystem model (CLASS-CTEM (Verseghy, 2012; Melton and Arora, 2016)) has been incorporated in the Modélisation Environmentale Communautaire (MEC) Surface and Hydrology system (MESH; (Pietroniro et al., 2007)) to integrate the MESH-CTEM modelling system. Although prior versions of MESH, herein referred to as MESH-CLASS, used CLASS to define land-surface processes, the incorporation of CLASS-CTEM provides additional ecological and biophysical parameterizations, such as carbon and feedbacks. The MESH-CTEM model was

calibrated and applied at the Big Creek watershed in Southern Ontario, Canada from October 1st 2004 to December 2017 to evaluate its performance and explore impacts environmental processes.

## 2. Methods

### 2.1 Model Description

The current MESH modelling system was first developed by Pietroniro and Soulis (2003) for the Mackenzie GEWEX program. It was then integrated with Environment and Climate Change Canada's Modélisation Environnementale Communautaire (MEC) community model and renamed 'MESH' (MEC – Surface and Hydrology) to emphasize its coupling of hydrological and land-surface processes at a watershed-scale (Pietroniro et al., 2007). The version of MESH used for this research (r1221) adds the 'WATROF' algorithms (Soulis et al., 2000, 2011) that have added topographic slope to the land surface column, an enhanced algorithm for overland flow, and lateral subsurface interflow, to the Canadian Land Surface Scheme (CLASS; version 3.6) and couples this with the distributed two-dimensional river channel flow routing algorithm, called WATROUT, found within the Waterloo Flood Forecasting Model (WATFLOOD) and its WF_ROUTE configuration (Kouwen, 1988). WATFLOOD is a numerical hydrological model which was developed to simulate hydrological processes within a watershed with an emphasis on streamflow forecasting including major flooding events for watersheds ranging from 100 $km^2$ to 10,000 $km^2$ in area (Kouwen, 1988). MESH uses WATFLOOD's algorithms to simulate streamflow using a one-directional drainage approach where a portion of the accumulated soil and surface water within each spatially defined grid cell drains into a single neighbouring cell. The direction of flow from a spatially defined grid cell in WATFLOOD follows the commonly used eight direction (D8) flow model developed by Jenson and Domingue (1988). (1988). This WAT- CLASS/MESH configuration has been used extensively in other watershed-scale simulations involving MESH (Haghnegahdar et al., 2014; Mekonnen et al., 2014; Xu et al., 2014; Haghnegahdar et al., 2015; Alavi et al., 2016).

CLASS (Verseghy, 2012) was originally developed for use as the land surface scheme in the global and regional climate models of Environment and Climate Change Canada. CLASS includes a single layer vegetation canopy and represents surface-atmosphere radiative and

turbulent (sensible and latent heat) exchanges, soil thermal properties, the soil water budget as well as snow on the ground and canopy (Bartlett et al., 2006) at a fine temporal (30 minutes) resolution. The current version of CLASS (v 3.6) incorporated into MESH, includes the addition of a variable soil permeable depth, organic soil layers and improvements to many of its thermal and hydrological algorithms (Verseghy, 2012). To represent spatial heterogeneity, CLASS is parameterized using GRUs (Grouped-Response Units), which are the sub-category of spatial grid cells. GRUs have no unique spatial component within their respective spatially defined grid cell but are rather considered to be a weighted fraction of the land-cover usage within the cell (Kouwen et al., 1993; Soulis et al., 2000). Furthermore, within each GRU is a weighted distribution of the different land use categories, which are parameterized as plant function types (PFTs). PFTs serve as the functionality of the basic vegetation algorithms within CLASS. Excluding the mixed forest land-use category, all GRUs contain only one dominating PFT. The four PFTs in CLASS excluding urban land-use, are: needleleaf trees (NL), broadleaf trees (BL), crops (CR) and grasslands (GR) (Verseghy et al., 1993). Urban areas are treated very similarly to vegetated areas, but they are assumed to be areas of bare soil with a high roughness length. Although CLASS simulations have traditionally employed three layers (Verseghy, 1991; Soulis et al., 2000; Pohl et al., 2005; Huang et al., 2011), this study used a total of six layers with respective thicknesses of 10, 25, 25, 25, 25 and 300 cm. Using multiple soil layers in the root zone helps to improve the model's dynamic root system processes as well as the soil water regime. Without WATROF, soil water could only leave the GRU through overland runoff, evapotranspiration, or drainage at the bottom of the soil column (Snelgrove, 2002). When CLASS is coupled with WATROF, additional algorithms are used to simulate sloped overland runoff and runoff from lateral interflow from the individual soil layers (Soulis et al., 2000; Snelgrove, 2002). The lateral flow components introduced by WATROF are (1) overland flow ($q_{\mathrm{Over}}$), the excess water at the surface moving towards the streamflow network in the grid cell, and (2) interflow ($q_{\mathrm{Int}}$), the lateral subsurface flow. Both components consider the impact of topographic slope. The calculations for each of these additional components are derived from Soulis et al. (2000), and are respectfully described by the following set of equations:

$$q_{Over} = \frac{2D_D}{n} d_e^{\frac{5}{3}} \sqrt{\Lambda_I} \quad (1)$$

$$q_{Int} = 2D_D K_{S0}(\Theta_S) \left(\frac{\Theta_1 - a\Theta_S}{\Theta_c - a\Theta_S}\right)^f \frac{D}{e+1} \Lambda_I \quad (2)$$

Where, $D_D$ is the drainage density, $K_{S0}$ is the horizontal saturated hydraulic conductivity at the surface, $n$ is manning's roughness coefficient, $\Theta_S$ is the saturated volumetric water content, $d_e$ is the depth above the ponded water, $f$ is an exponent, $D$ is the depth the soil layer, $e$ is an exponent normally between 1 and 5 and $\Lambda_I$ is the topographic slope of the GRU. Equation (2) is a re-parameterization of the Richard's equation for unsaturated flow in a porous media (Richards, 1931). The one-dimensional vertical structure of CLASS has been retained for thermal exchanges. Therefore, all thermal-related properties within a GRU are independent of other GRUs. The estimates of snowfall are accomplished by partitioning incoming precipitation into snowfall and rainfall using empirically derived equations. This study assumed that any precipitation falling below an air temperature of 0 $^{o}$C would be assumed as snow.

As mentioned earlier, in this study, the coupled CLASS-CTEM (Canadian Land Surface Scheme - Canadian Terrestrial Ecosystem Model; Melton and Arora, 2016) was incorporated into MESH as a new land-surface model. Figure (1) provides visualization of the key physical and biogeochemical processes and interactions of MESH with CLASS-CTEM. The WATROF algorithms represented by equations (1) and (2) were preserved from MESH with CLASS (v 3.6) into CLASS-CTEM. A unified modelling language (UML) diagram visualizing MESH-CTEM's coded structure including input and output files is given in Figure (2). This implementation of MESH with CLASS-CTEM allows users to turn-off its CTEM algorithms such that MESH is able to use updated version of CLASS (v 3.6.2) included with CTEM instead of the older version (v 3.6) currently distributed with its code. For comparison

purposes to assess only the impact of adding the ecological and biophysical components added by CTEM to MESH, simulations referred to 'MESH-CLASS' will be using the updated version of CLASS (v 3.6.2) available by CLASS-CTEM but with all CTEM algorithms turned off. Simulations referred to 'MESH-CTEM' will be using CLASS-CTEM with its CTEM algorithms turned on.

CLASS-CTEM itself is a coupled model which incorporates CLASS's land surface parameterizations but adds photosynthesis, a carbon cycle and dynamic vegetation capability through coupling with CTEM (Canadian Terrestrial Ecosystem Model; Arora and Boer, 2005; Melton and Arora, 2016). CLASS-CTEM is used as the land surface model in the Canadian Earth System Model (CanESM) (Arora et al., 2009; Shao et al., 2013).

Being a dynamic vegetation model, the functionality of this CTEM version is to simulate carbon processes such as photosynthetic productivity, respiratory fluxes in both soil and vegetation and the distribution of carbon into different carbon pools with respect to its nine PFTs (Arora, 2003; Arora and Boer, 2005). Version 2.0 of CTEM is described extensively in Melton and Arora (2016). CTEM simulates all of its processes on a daily time scale, the only exception being modelled photosynthesis which is calculated on the timestep of CLASS (usually 30-minutes). There are five carbon pools within CTEM, with three being live (leaves, stem and roots) and two dead (litter and soil carbon). Net ecosystem productivity (NEP) is the net difference between gross ecosystem productivity (GEP) and ecosystem respiration (Re). The CLASS PFTs correspond to the CTEM PFTs as follows the needleleaf trees are divided into their evergreen (NDL-EVG) and deciduous sub-types (NDL-DCD), broadleaf trees are divided into their evergreen (BDL-EVG), cold-deciduous (BDL-DCD-COLD) and drought-deciduous sub-types (BDL-DCD-DRY), crops into C3 (C3-CROP) and C4 (C4-CROP) sub-types, and grasses into their respective C3 (C3-GRASS) and C4 (C4-GRASS) sub-types. Default CLASS uses the Jarvis-Stewart method to estimate canopy resistance ($r_c$) (Jarvis, 1976). However, CLASS-CTEM is designed to calculate $r_c$ using either the Ball–Woodrow–Berry (BWB) model (Ball et al., 1987) or the Leuning model (Leuning et al., 1995). For this research, the Leuning model will be applied, which calculates $r_c$ with the following function:

$$r_c = \left( m \frac{A_{nP}}{\mathbb{f}(c_s - \Gamma)} \frac{1}{\left(1 + \frac{D}{D_0}\right)} + bL_T \right)^{-1} \quad (3)$$

where $m$, $b$ and $D_0$ are vegetation dependent parameters, $A_n$ is net canopy photosynthesis rate, Γ is the $CO_2$ compensation point, $D$ is the vapour pressure deficit and $L_T$ is the total LAI (Leaf Area Index). Rooting depth for each PFT in CTEM is calculated based on their respective available root biomass and the estimated root density decreases exponentially in the soil column (Arora and Boer, 2003).

Later on, Huang et al. (2011) incorporated N cycling in the model to develop CLASS-CTEM-N+ model. It includes biological fixation and soil mineralization, nitrification and denitrification routines to simulate N constraints on carbon cycling in vegetation ecosystems (Huang et al., 2011). CLASS-CTEM-N+ has been test at both site-level and global scales (Huang et al., 2016a; Huang et al., 2016b).

In addition to the carbon fluxes and dynamic vegetation simulations, integrated MESH-CTEM includes nitrogen cycling algorithms as well following Huang et al. (2011) and Huang et al., (2016a, b). However, due to limited observed data for certain PFTs, nitrogen components were turned off for the MESH-CTEM simulation in the Big Creek watershed.

### 2.2 Study Area

The MESH-CTEM model was tested at the Big Creek watershed in southern Ontario, Canada from October 2004 to December 2017 using observed eddy covariance flux, meteorological, biometric and hydrologic data (Figure 3). Big Creek watershed is a 573 $km^2$ crop-dominated catchment with significant coverage of broadleaf and needleleaf forests. Although numerous MESH research projects have used watersheds with an area larger than 1000 $km^2$ (Pietroniro et al., 2007; Mekonnen et al.; Haghnegahdar et al., 2014, 2015; Yassin et al., 2017), using a relatively smaller watershed in this study was preferred due to the limited availability of biometric, energy, water and carbon flux data and initialization values for CTEM's carbon

pools and other vegetation parameters. Furthermore, using the slope estimation algorithm described by Burrough and McDonnell (1998), the area was characterized to be relatively flat with a mean slope incline of 2.05 %, with a standard deviation of 2.17 %.

Using the 2010 30 m land-use dataset from Latifovic et al. (2017), the land-use distribution of Big Creek watershed is given in Table 1, with the majority of the land mainly being cropland. The main crops growing within the watershed are soybeans (*Glycine max*), corn (*Zea mays L.*) and mixed grains, although precise annual numbers vary (Long Point Region Conservation Authority, 2008). Most of the forest cover within the watershed are planted stands over previous farmland that was cleared in the early 20$^{th}$ century (Zavitz, 1961). During the 1910s for example, only 10 % of Norfolk county including the Big Creek watershed was forested (Richardson, 1953), but this has increased to 25 % presently through various plantation programs implemented in the 1940s and 1950s to combat soil degradation. Furthermore, the watershed is relatively homogeneous in soil texture with approximately 90 % of the watershed being covered by the Norfolk sand plain, while the remaining areas are covered by the Haldimand Clay plain; primarily in the south closer to the shores of Lake Erie (Chapman and Putnam, 1984; Long Point Region Conservation Authority, 2008). The only urban settlement is the hamlet of Delhi, with a population of 4,172, while numerous rural homes are also scattered within the basin, (Statistics Canada, 2012).

Observed flux and biometric data from two nearby Global Water Futures (GWF) Program's Turkey Point flux observatory sites were used in this study (Figure 3), TP39 (42.71 $^{o}$N, 80.35 $^{o}$W) and TPD (42.63 $^{o}$N, 80.55 $^{o}$W), registered with FluxNet Canada under CA-TP4 and CA-TPD respectively. TP39 is a monoculture pine plantation forest planted in 1939 with partial thinning treatments in 1983 and 2012 (Peichl and Arain, 2006; Peichl et al., 2010). TPD is about 90-year old deciduous forest with dominant tree species of white and red oak (*Quercus alba* and *Q. Rubra*) (Kula, 2013; Beamesderfer et al., 2019). Initialization parameters for TP39 and TPD sites are given in Table 2. Energy, water and carbon flux measurements have been taken at TP39 since 2003 and at TPD since 2012 using eddy covariance systems (Peichl et al., 2010; Beamesderfer et al., 2019). Observed energy flux data from crops were obtained from the Elora FluxNet site (43.65 $^{o}$N, 80.42 $^{o}$W). Crops planted at Elora were corn for 2005, 2007, 2016 and 2017, while soybeans were planted in 2006. Carbon flux values from a corn site were gathered from FluxNet's US-IB1 site (41.86 $^{o}$N, 88.22 $^{o}$W).

According to the Köppen climate classification scheme, this area is mostly comprised of a humid continental climate (Peel et al., 2007). Based on a 30-year average of observed weather data (1981 - 2010) from the Delhi Hydrometric Station (42.87 $^{o}$N, 80.55 $^{o}$W), mean monthly temperature range from 21.1 $^{o}$C in July to -9.1$^{o}$C in January with a mean annual temperature of 8.0 $^{o}$C. The average precipitation falling at Delhi over that same 30-year period is 1036 mm year$^{-1}$. The average monthly streamflow of Big Creek recorded at ECCC's Walsingham Hydrometric station (42.68 $^{o}$N, 80.54 $^{o}$W) ranges from 7.8 m$^3$ s$^{-1}$ in March to 2.6 m$^3$ s$^{-1}$ in September.

Figure (4) provides an illustration of the observed forcing data used in the model. Some notable weather periods were observed over the 2004-2017 study period, such as a summer drought in 2007, a warm period in the 2005-2006 winter and significant high streamflow events during the winter of 2008-2009.

### 2.3 Model Parameters and Forcing Data

The input data required for MESH-CTEM are the meteorological forcing data, CLASS-specific surface and soil parameters, hydrological-specific parameters, a drainage database containing the data pertaining to the watershed, and initial values with respect to temperature, soil water content and snow depth.

The simulation for Big Creek does not require an ultra-high resolution for its spatial grids as there is a lack of small-scaled streamflow variability due to a relatively flat terrain. Given the catchment's size and topography, the resolution chosen for the drainage database grids is ~2.7 km$^2$ (0.02$^{o}$ latitude x 0.02$^{o}$ longitude). There are 210 active grid cells being simulated with 209 assumed to be within the basin area. The land-use information given to these grids was the data set provided by Latifovic et al. (2017) which had a resolution of 30 m x 30 m and is considered representative of land-use in 2010. All land-use data were then converted into the weighted distribution of land-cover for each 2.7 km$^2$ grid cell. With a total of nine land-use categories excluding waterbodies, each of the CLASS and CTEM PFTs were defined using this land-use data set. Furthermore, the watershed delineation process described by Jenson and Domingue (1988) was used to define the watershed area of Big Creek draining towards the Walsingham Hydrometric Station. The Digital Elevation Model (DEM) used for the

delineation process was provided by Natural Resources Canada (NRCan) with a resolution of 3/4 arc-seconds (approximately 22.5 m). This DEM was also used to derive elevation and slope for the drainage database file. Because of the simulated area being relatively small and due to the homogeneity among the different land-use types, the same sets parameters and initial conditions were assigned to each representative grid cell to its respective GRUs as shown in Table (1). Finally, for the drainage data it was assumed that there is only one river class parameterization for routing parameters for the whole domain.

CTEM also calculates stomatal resistance values such that associated parameters in CLASS used to calculate previously used to calculate stomatal resistance are no longer used. For the default MESH simulations using CLASS as its land surface model, the Jarvis-Stewart parameterization method was employed. For the MESH-CTEM simulations the canopy resistance was calculated with respect to photosynthesis using equation (3). Initial values for all six of its carbon pools were provided from the observations made at the nearby Fluxnet tower sites as described in Table (2). Only five CTEM PFTs were assumed to be present in the Big Creek watershed. These PFTs include NDL-EVG (Needleleaf Evergreen) BDL-DCD-COLD (Broadleaf Deciduous Cold), C3-CROPS (C3 Crops), C4-CROPS (C4 Crops) and C3-GRASS (C3 Grasses). The only major change to the internal parameters within CTEM were those related to crop harvest and changes to the photosynthesis temperature ranges. By default, crops are harvested once a certain temperature threshold is reached or when Leaf Area Index (LAI) has reached some threshold. In order to more accurately simulate the timing of the harvest given modelled growth, the maximum LAI before a simulated harvest was change from 3.5 and 4.5 $m^2\ m^{-2}$ to 1.0 and 3.5 $m^2\ m^{-2}$ for C3-CROPS and C4-CROPS respectively. The upper and lower temperature limits of photosynthesis were also changed for the forest PFTs to reflect observations made at TP39 and TPD.

The initial soil temperature and water content in all three layers were estimated from observations made at TP39 on October 1$^{st}$ 2004 and given to the needleleaf and broadleaf GRUs. The initial water content for the crops GRU was set relatively higher to reflect the streamflow a few days into the simulation. For the three layered simulations, layers one to three were initialized using observations at depths of 5 cm, 20 cm and 100 cm respectively averaged from two separate observation points. For the six layer simulation, the bottom four layers were given all the same initial condition in order to replicate the three layer initialization

values.

Finally, the forcing data used in the model includes incoming shortwave radiation, incoming longwave radiation, air temperature, specific humidity, wind speed, precipitation, and barometric pressure. This forcing data was obtained as gridded average values for each model grid-cell across the watershed at an hourly time scale. With the exception of precipitation, all forcing data were gathered from the Regional Deterministic Prediction System (RDPS) from ECCC (Mailhot et al., 2006). The precipitation data were obtained from Canadian Precipitation Analysis (CaPA) (Mahfouf et al., 2007). RDPS data was inputted at an hourly temporal scale but was averaged to a 30-minute scale when used within CLASS. The CaPA model outputs were in a 6 hour temporal with each CLASS 30-minute iteration using the same precipitation rate within a 6 hour period. The meteorological and precipitation data used in the model were cross-checked with precipitation data from flux tower site locations. In terms of spatial variability between grid-cells for the forcing data, the data were relatively homogeneous as the standard deviations are relatively small. As a measurement of spatial variability of the forcing data, the mean of the spatial average deviations from the spatial mean are 0.46 $C^o$ for temperature, 2.67 mm $day^{-1}$ for precipitation $1.8 \cdot 10^{-4}$ kg $kg^{-1}$ for specific humidity, 8.4 W $m^{-2}$ for incoming shortwave radiation, 5.3 W $m^{-2}$ for incoming longwave radiation, 0.12 m $s^{-1}$ for horizontal wind speed and 231.9 Pa for atmospheric pressure. The streamflow data at the Walsingham Hydrometric Station were recorded by ECCC and accessed from the Water Survey of Canada National Water Data Archive (https://wateroffice.ec.gc.ca/mainmenu/historical_data_index_e.html). The extracted streamflow data were aggregated to a daily time-scale.

## 2.4 Model Calibration

An automatic calibration process was applied to the default MESH simulation (MESH-CLASS) to find the best parameter values for GRUs in the Big Creek catchment using the Dynamically Dimensioned Search (DDS) algorithm (Tolson and Shoemaker, 2007). Because of the ability of DDS to calibrate a large number of parameters within multi-scale distributed hydrological models, DDS has been a popular option for calibrating MESH simulations (Dornes et al., 2008; Haghnegahdar et al., 2014; Davison et al., 2016). The calibration was performed using the Ostrich optimization and calibration software (Matott, 2017).

DDS attempts to find the best set of model parameters by running a simulation several times, providing a candidate parameter solution for each simulation. The only parameter needed for the calibration algorithm was a scaler perturbation parameter determining the change of parameters between calibration simulations, which was set to 0.2 as recommended by Tolson and Shoemaker (2007). A total of 200 simulations were used for the calibration process which was the total number of simulations used before the DDS algorithm converged to a solution with respect to its objective function. In terms of assessing and testing model performance, a given set of parameters was compared to the current and best parameter solution by a user-defined objective function. The objective function for this calibration process was the Nash-Sutcliffe efficiency (NSE) index (Nash and Sutcliffe, 1970) of simulated vs observed daily streamflow at Walsingham Hydrometric Station. With respect to our simulation, NSE was calculated as:

$$NSE = 1 - \frac{\sum_{i=1}^{n}\left(Q_i^{obs} - Q_i^{sim}\right)^2}{\sum_{i=1}^{n}\left(Q_i^{obs} - \overline{Q^{obs}}\right)^2} \quad (4)$$

where $i$ is the current simulated day, $n$ is the number of observations, $Q^{\text{obs}}$ is the observed volumetric streamflow, $Q^{\text{sim}}$ is the simulated streamflow and $\overline{Q^{obs}}$ is the mean of the observed streamflow. The benefits of calibrating MESH with respect to streamflow have been well-documented (Haghnegahdar et al., 2014, 2015; Yassin et al., 2017). However, for model inter-comparison purpose, final MESH and MESH-CTEM simulations were performed using 6-soil layers and the same set of initial parameters as derived using Default MESH model and DDS methods. Findings of model inter-comparison are described in the results section. In order to limit the number of parameters being calibrated, the needleleaf and broadleaf calibrated hydrological parameters were grouped together, as well as crops and grasslands. Additionally, the ranges for the calibration parameters excluding soil texture parameters were based on ranges from previous MESH calibrations from the great lakes region (Haghnegahdar et al., 2014). Calibrated soil texture parameters were restricted to ranges associated with sandy soils due to the known local soil characteristics and previous simulations using CLASS-CTEM (Huang et al., 2011).

## 2.5 Statistical Analysis

In order to compare the outputs of MESH-CLASS and MESH-CTEM with observed data, a number of statistical methods were used. Equation (4) was used to estimate the accuracy of simulated carbon (Huang et al., 2011).

For measuring the errors, Mean Absolute error (MAE) and Root Mean Square Error (RMSE) were used as described below:

$$RMSE = \sqrt{\frac{1}{n}\sum_{i=1}^{n}(P_i - O_i)^2} \tag{5}$$

$$MAE = \frac{\sum_{i=1}^{n}|P_i - O_i|}{n} \tag{6}$$

Where $n$ is the total number of observations, $P_i$ is an estimated value at time $i$ and $O_i$ is an observed value at time $i$. An $F$-test was calculated for the respective simulations using the following:

$$F = \frac{\sum_i^n \left(y_i - f_1(x_n)\right)^2}{\sum_i^n \left(y_i - f_2(x_n)\right)^2} \tag{7}$$

where $y_i$ is the observed value while $f_1(x_i)$ and $f_2(x_i)$ are the estimated/modelled values given the input $x_i$ at time $i$.

# 3. Results

## 3.1 Calibrations

The resulting parameters from the DDS calibration process are given in Table (3) along with the simulated streamflow from both the MESH-CLASS and MESH-CTEM models for 6-soil layer formulations compared to the observed values at the Walsingham hydrometric station (Figure 5). Comparisons for simulated monthly averaged streamflow versus observations from

3- and 6-soil layer model formulations are shown in Figure (6). A summary of the streamflow results including parameter values for their respective GRUs is given in Table (4). MESH-CTEM had a much larger total annual discharge, with the total water contributing to streamflow increasing by 72 % and 42 % for the 3- and 6-soil layered model simulations. For the 3-soil layer simulations, the NSE value of MESH-CLASS was -0.16, while MESH-CTEM had an NSE value of 0.43 for respective streamflow ranges of 0.1 to 37.5 $m^3 s^{-1}$ and 0.35 to 37.2 $m^3 s^{-1}$. For the 6-soil layer simulations, the MESH-CLASS NSE value was 0.12 and the MESH-CTEM NSE was 0.38, with respective streamflow ranges of 0.35 to 49.6 $m^3 s^{-1}$ and 0.35 to 39.13 $m^3 s^{-1}$.

Overall, MESH-CTEM did well in estimating streamflow at the Walsingham Hydrometric Station over the 13-year period. Furthermore, the periods of low flow were significantly improved, such as the summers of 2007, 2010 and 2016. However, MESH-CTEM still slightly underestimated these low flow periods and both models were unable to accurately simulate high streamflow events such as the spring melting events of 2009, 2011 and 2016 and the large spikes in streamflow during the winter of 2008-2009.

### 3.2 Hydrological Processes

Comparisons of monthly mean observed and simulated volumetric water content (VWC) in soil layers in the NDL-EVG PFT as well as modelled snow cover are shown in Figure (7). Observed VWC was measured at 5, 20, 50 and 100 cm and averaged from two different measurement locations at TP39 approximately 30 m away from each other. With respect to those observational depths, MESH-CTEM was able to simulate VWC quite well for soil layers (e.g. $VWC_1$, $VWC_2$, $VWC_3$ and $VWC_5$ in Figure 7) with respective $R^2$ values of 0.17, 0.42, 0.64 and 0.40. Furthermore, the addition of CTEM into the soil-water regime did noticeably change VWC in all layers in terms of overall magnitude and patterns. Surprisingly, the most noticeable and significant modelled change was for $VWC_5$, where there was a significant increase of soil water for nearly the entire simulation period. For the upper layers however, the most significant changes to VWC were mostly during periods of drought. For instance, the mean difference in simulated daily mean VWC between MESH-CLASS and MESH-CTEM simulations for all six layers is 0.006, 0.010, 0.011, 0.022, 0.032 and 0.042 $m^3 m^{-3}$,

respectively. Using equation (7), the overall difference in the daily mean values of the simulated VWC by both models are all significant with $p < 0.01$. During droughts and when the soil is near the minimum residual soil water content (VWC = 0.04), MESH-CTEM was able to retain more water than MESH in its upper layers such that wilting point is often delayed by a few days. For example, the changes in $VWC_1$ before the soil hits pre-defined wilting point minimum residual soil water content are the most significant changes (Figure 7). Due to the unrealistic and brief time period of the percent of frozen water within the soil simulated by MESH-CTEM, modelled frozen water content is not shown in Figure (7).

The differences between MESH-CLASS and MESH-CTEM simulated components of lateral soil water flow ($q_{Int}$) and drainage from the bottom of the soil ($q_{Base}$), and water loss through transpiration for all four CLASS PFTs within the respective GRUs ($QFC_n$) for the entire simulation period (13 years) is shown in Table (5). Although there were some periods of simulated overland flow, their overall contribution to the soil water regime was insignificant ($p > 0.05$). The differences between MESH and MESH-CTEM simulated components of lateral soil water flows ($q_{Base}$ and $q_{Int}$) and water loss through transpiration for all canopy layers ($QFC_n$) for all four CLASS PFTs for the entire simulation period (13 years) is shown in Table (5). Although there were some periods of simulated overland flow, their overall contribution to the soil water regime was insignificant ($p > 0.05$). When activating CTEM with respect to a calibrated MESH, There was a noticeable increase in interflow and baseflow for all PFTs except a slight decrease in interflow for NDL-EVG. For transpiration, there were a number of changes for each canopy layer for each PFT (Table 5). Overall, there was not any significant change in the transpiration loss from the first soil layer for the forested PFTs ($QFC_1$). The crops and grass PFTs had a much more dramatic decrease in $QFC_1$. Values of QFC below the first canopy layer experienced a noticeable decrease for all PFTs.

Time series of the daily mean values of latent heat ($Q_E$) and Sensible heat ($Q_H$) fluxes simulated by MESH-CLASS and MESH-CTEM for each of the major CLASS PFTs and the subsequent CTEM PFTs in the catchment and observed $Q_E$ from forest sites (TP39 and TPD as daily means) and crops (Elora station as monthly ensemble means) are shown in Figure (8) and (9) respectively. Note that the Crops PFT in the MESH-CTEM simulation is separated into their respective C3 and C4 classifications. Comparison of MESH-CTEM's monthly mean values of $Q_H$ and $Q_E$ in energy fluxes for the forest PFTs against observations at TP39 and

TPD are shown in Figure (10). The decrease in $Q_E$ by MESH-CTEM was significant for a paired t-test with $p < 0.01$. These decreases occurred year-round for all PFTs. The annual average values of $Q_E$ for the MESH-CLASS and MESH-CTEM models were 63.8 to 47.6 W $m^{-2}$ for needleleaf forests; 63.4 to 43.5 W $m^{-2}$ for the broadleaf forests; 38.0 to 25.8 W $m^{-2}$ for crops and 45.1 to 32.6 W $m^{-2}$ for grasses. Similarly, C3-CROPS had an overall annual increase ranging from 28.3 to 23.6 W $m^{-2}$. However, the change in $Q_H$ in crops is not as dramatic as in the forested PFTs and there were a few years where $Q_H$ experienced an overall decrease. C3-GRASS was the only PFT where annual $Q_H$ flux decreased every year from 53.3 to 30.4 W $m^{-2}$. The annual $Q_H$ for the forest PFTs seems to have a net increase from the MESH-CTEM, ranging from 36.9 to 56.4 W $m^{-2}$ for NDL-EVG and 20.4 to 35.1 W $m^{-2}$ for BDL-DCD-COLD. These changes in $Q_E$ and $Q_H$ created more realistic simulations given observations at TP39 and TPD sites. Observed annual fluxes seen for $Q_H$ at TP39 and TPD was 30.9 and 24.3 W $m^{-2}$ respectively, while the $Q_E$ at the same sites was 35.6 and 29.9 W $m^{-2}$. Although annual energy fluxes at TPD might be more relatively accurate, the relatively large variabilities seen in Figures (8), (9) and (10) make it more difficult to estimate than TP39 on a monthly and daily time scale.

A summary of monthly accuracy of evapotranspiration at the TP39 forest site with respect to both models is given in Table (6). The MAE and RMSE decreased for all months once CTEM was implemented in MESH-CLASS. The simulated ET by the MESH-CTEM decreased for each month and average annual ET was only 12.6% higher than the observed ET value. A paired *F*-test showed that MESH-CTEM significantly decreased overall annual ET while increasing accuracy as compared to the observed evapotranspiration values with $p < 0.01$. Over estimation of evapotranspiration by MESH-CTEM occurred mostly during the winter months. The summer and autumn months were relatively accurate with some months slightly underestimating ET. These seasonal patterns were very similar to those shown for BDL-DCD-COLD simulations and the comparisons made at TPD (Table 6). Furthermore, the periods of low flow were significantly improved, such as the summers of 2007, 2010 and 2016. However, MESH-CTEM still slightly underestimated these low flow periods.

### 3.3 Carbon Fluxes

MESH-CTEM simulated daily mean carbon fluxes and observed fluxes for the NDL-EVG and

BDL-DCD-COLD PFTs are shown in Figure (11). A monthly scatter plot of the same fluxes including their respective monthly RMSE and NSE values are shown in Figure (12). Even when averaged on a monthly time scale, Figure (12) shows the relatively larger variability of carbon fluxes for the deciduous simulations as compared to the evergreen simulations. On a daily scale, the simulated GEP, Re and NEP for the NDL-EVG PFT had estimated NSE values of 0.79, 0.82 and 0.38, respectively. The mean annual values of simulated fluxes for the same three components over 2005 to 2017 period were 1456, 1239 and 217 g C $m^2$ $yr^{-1}$, respectively. In contrast, the observed mean annual GEP, Re and NEP values before the thinning event of 2012, which was not represented in the model, were 1411, 1244 and 167 g C $m^{-2}$ $yr^{-1}$, respectively, with the respective mean daily values ranging from 0.001 - 11.15 g C $m^{-2}$, 0.95 - 8.34 g C $m^{-2}$ and -3.20 - 4.48 g C $m^{-2}$ respectively. For the fluxes within the BDL-DCD-COLD PFT, the mean annual values of simulated fluxes were respectively 1257, 1048 and 208 g C $m^2$ $yr^{-1}$, while the observed fluxes at the TPD site were 1347, 1184 and 163 g C $m^2$ $yr^{-1}$ respectively. A lot of the underestimations of NEP can be attributed to the relatively large decrease of GEP during drought years such as 2007 and 2016. It appears that CTEM's decreasing rate of GEP is more sensitive to relatively severe inter-annual droughts than what was observed at the FluxNet sites. However, estimations of carbon fluxes are much more accurate during non-drought years.

Cumulative values of NEP for all study years (2005 to 2017) are shown in Figure (13). The annual mean NEP for each PFT over the study period is 200, 209, -10, 60 and 97 g C $m^{-2}$ for NDL-EVG, BDL-DCD-COLD, C3-CROPS, C4-CROPS and C3-GRASS, respectively. The forest and grass NEP values reflect the total changes in all five active carbon pools summed together. However, C3-CROPS and C4-CROPS experienced a complete removal of their stem, root and leaf carbon pools in winter as expected. Because of this most of the annual changes in NEP for both crop PFTs were due to changes in their litter and soil carbon pools. While most years experienced positive NEP for all PFTs, the least productive years for all PFTs were the drought years such as 2007 and 2016.

An ensemble summary of the NEP fluxes within the different PFTs compared to available data for all simulation years (2005-2017) is shown in Figure (14). The daily mean GEP ranged from 0.004 to 11.2, 0.0 to 15.1, 0.0 to 5.42, 0.0 to 28.5 and 0.0 to 8.47 g C $m^{-2}$ $yr^{-1}$, while the $R_e$ ranged from 0.95 to 8.35, 0.59 to 8.01, 0.13 to 2.28, 0.45 to 11.1 and 0.43 to 4.8 g C

$m^{-2}$ $yr^{-1}$ for EVG-NDL, BDL-DCD-COLD, C3-CROPS, C4-CROPS and C3-GRASS respectively.

### 3.4 Catchment-scale budgets

On average, contribution to NEP flux for the land use categories of needleleaf, broadleaf, mixed, crops and grassland for the entire basin was approximately 0.4 %, 27.8 %, 15.7 %, 1.1 % and 55.4 %, respectively. A mapped output of annual average $Q_H$, $Q_E$, $R_N$ (Net Radiation), GEP, Re and NEP over the Big Creek catchment for all model grids is shown in Figure (15). The model behaved as expected by estimating the largest exchanges of $Q_E$ for the forested areas, whereas areas with crops experienced relatively small $Q_E$. When taking the gridded average, the GEP, Re and NEP values from the basin were 660, 640 and 20 g C $m^{-2}$ $yr^{-1}$ respectively. While the gridded averages of $Q_E$, $Q_H$ and Net Radiation are 33, 27 and 60 W $m^{-2}$. The upper and lower ranges of grid outputs originated from grids which were relatively homogeneous. For example, the grid with the highest annual $Q_E$ (49 W $m^{-2}$) is also the grid with the highest concentration of the Broadleaf land-use type (78 %). In contrast, the grids on northern areas of the catchment are estimated to have lower $Q_E$ fluxes due to the relatively higher concentration of crops in that area.

## 4. Discussion

Calibration of MESH-CLASS using streamflow data from the Walsingham Hydrometric Station for the Big Creek catchment had a few limitations. For instance, the model was unable to adequately replicate high streamflow events, including a maximum daily value of 75.4 $m^3$ $s^{-1}$ experienced in the winter of 2008-2009. The high peaks during those winters were due to the high volume of snowmelt caused by unusually energy fluxes and high temperatures such as an observed daily mean temperature of 9.0 $^oC$ and a daytime high of 14.2 $^oC$ on December 27$^{th}$, 2008 (at TP39). Haghnegahdar et al. (2014) had described similar limitations while calibrating MESH streamflow for their Great Lakes basin simulations during this period due to the inability of the model to estimate the high melt of snow and ice. We also observed similar limitations while using MESH-CTEM in the Big Creek catchment where underestimation of peak streamflows are consistent with an underestimation of snow cover

and in turn, an underestimation of snow melt. Furthermore, 73.8 % of the Big Creek catchment was covered by crops. This dominance would have caused some limitations in the calibration as having a crop dominant GRU for a single basin calibration strategy has been found to perform less accurately than having a more equal distribution of multiple land-use types (Haghnegahdar et al., 2014). Furthermore, streamflow may also have been changed due to an underrepresentation of irrigation processes within the crop areas in the region. Specifically, CLASS-CTEM currently only represents crop irrigation by reducing the crops moisture stress. Despite the difficulty of determining how irrigation processes contribute to changes in streamflow in the Big Creek watershed, it is very likely that irrigation schemes within the watershed have been decreasing streamflow with significant decreases of summer flows as most water is pumped in the summer from streams or human constructed ponds within the watershed that contribute in reducing streamflows (Long Point Region Conservation Authority, 2008; Shortt et al., 2009). Although there was no significant change between the 3-layer and 6-layer models for MESH-CTEM, MESH streamflow estimates were significantly different between the 3-layer and 6-layer models. Volumes of $q_{Int}$ in the deepest layer during the 3-layer simulation of MESH-CLASS were relatively small given its relatively larger depth. However, adding more layers closer to the surface created a more continuous flow representation with respect to depth and thus contributed more to overall $q_{Int}$ and eventual streamflow. Since the deeper layers in MESH-CTEM already had relatively significant contributions of $q_{Int}$ in its 3-layer simulation and had more uniform values of $q_{Int}$ with respect to depth, the additional layers did significantly less in streamflow contribution.

Although MESH calibrations have generally focused on using streamflow and a single objective approach (Pietroniro et al., 2007; Haghnegahdar et al., 2014; 2015), multi-objective calibration approaches have gained much recognition recently including within the MESH user community (Davison et al, 2016, Yassin et al., 2017). A multi-objective approach should be considered if MESH-CTEM is calibrated for future studies as the accuracy of carbon fluxes and dynamic vegetation growth would not be fully represented, if a single-objective approach based on streamflow is used. A multi-objective calibration approach involving observed streamflow, evapotranspiration and net ecosystem productivity from flux towers should therefore be considered for future MESH-CTEM calibrations. In the literature, similar approaches have been used to calibrate ecohydrological models to simulate hydrological and

vegetative processes (Sinnathamby, 2014; Tang et al., 2018).

In this study, simulated streamflow by the MESH-CLASS and MESH-CTEM models was significantly different with MESH-CTEM having higher amounts of available water for lateral flow and streamflow. These underestimations in MESH-CLASS were largely due to use of static CLASS parameters used to calculate stomatal resistance. Although these set of CLASS parameters are preferably calculated in-situ at the modelled location (Verseghy, 1991, 2011), many CLASS and MESH simulations continue to use these generalized parameters in their initialization files (MacDonald, 2016; Davison et al., 2016; 2019) or by calibrating them (Davison, 2006; Dornes et al., 2008; Haghnegahdar et al., 2014, 2015; Kornelsen et al., 2016). Incorporation of CLASS-CTEM as a land surface model in MESH allowed an alternative method to estimate these parameters and simulated streamflows that were more realistic.

The changes in the soil water regimes for all PFTs in MESH-CTEM as shown in Table (5) indicate a shift in dominant flow mechanisms where a large portion of water regularly leaving the soil through transpiration was now being released as interflow or baseflow. This shift in the soil-water regime helped to explain the increase in streamflow and lower $Q_E$ values seen in Figures (7) and Figure (5), respectively. For the changes in VWC in our NDL-EVG PFT in Figure (7), the deepest layers saw more dramatic VWC changes due to changes in transpiration and baseflow shown in Table (5). Inaccuracies in the winter VWC in the upper layers can be explained by the freezing of soil water by CLASS. However the volumetric ice content of the soil was too large given the field capacity of the soil and observations. The upper soil layers in CLASS have been challenging for simulating VWC because of the unpredictable nature of the near-surface soil with respect to changes in temperature and water (Maheu et al., 2018).

When considering the hydrological simulations using MESH-CTEM, perhaps the most significant change introduced was the decrease in $Q_E$ or evapotranspiration. This decrease in $Q_E$ to more realistic levels brought about increases in modelled streamflow, energy fluxes and volumetric soil water content. A change from the Jarvis-Stewart to Leuning canopy resistance/conductance formulation helped in decreasing overall $Q_E$ as there were decreases in the modelled canopy transpiration. Having the option to use the Leuning method in CTEM also helped in improving estimates of canopy resistance ($r_c$), as the limitations of

the traditional Jarvis model have been well documented (Damour et al., 2010; Gerosa et al., 2012; Buckley et al., 2017). There was a slight overestimation of $Q_E$ in MESH-CTEM (Figures 8 and 10) as compared to observations for the conifer forests, which was not surprising as it has been observed by other studies (Huang et al., 2011, 2016b; Wu et al., 2016). When compared to default MESH, MESH-CTEM's simulated $Q_E$ values for deciduous forests (BDL-DCD-COLD PFT) fell by 23%, with annual evapotranspiration at 594 mm $yr^{-1}$ (Figure 10). Even with this dramatic decrease, this was still an overestimation given observed annual evapotranspiration value of 450 mm $yr^{-1}$ from 2012-2016 at TPD. These overestimations have been previously observed for deciduous forest simulations in North America (Huang et al., 2016b; Asaadi et al., 2018). MESH-CTEM showed a 47 % decrease in annual evapotranspiration for crops when compared to MESH-CLASS, however, such comparisons can be difficult due to the variations of energy budgets between different $C_3$-crop types (Kelliher et al., 1995; Suyker and Verma, 2009). Unlike other land-use types, the annual evapotranspiration cycle changed dramatically for the crops as there was a noticeable annual spike in evapotranspiration in mid-summer due to the presence of mature $C_4$ crops. Nevertheless, the simulated mean annual evapotranspiration values for the crops by MESH-CLASS and MESH-CTEM were 320 and 608 mm $yr^{-1}$, respectively. By further subdividing the four PFTs of CLASS to nine used in CTEM, the energy simulations are able to be more representative by using algorithms more specific to their species. These specifications are important due to the large differences in energy budgets within needleleaf forests (Hamada et al., 2004), broadleaf forests (Zhou and Wang, 2016) and $C_3$/$C_4$ crops and grasses (Abraha et al., 2016). Addition of wetlands and shrublands is recommended for future MESH-CTEM simulations (Wu et al., 2016), especially when the simulated watershed contains a significant coverage of wetlands or ponds, which would help to regulate streamflow and flooding (Martinez-Martinez et al., 2014; Pattison-Williams et al., 2018). In essence, the changes in the energy budget is one example of how incorporation of CTEM in MESH helps in developing less generalized representations of ecosystems and flora in the model.

For the carbon flux results, MESH-CTEM did an excellent job in simulating GEP, Re and NEP at the TP39 site as shown in Figure (11). The annual and monthly values were very similar to the observed and previously analyzed patterns at this confer forest site (Huang et al., 2011; Trant, 2014). The carbon fluxes for all other PFTs shown in Figure (14) vary in

terms of magnitude and timing; however, they are similar to observed fluxes at TP39, TPD and US-IB1 sites. Similar trends were shown by previous CLASS-CTEM studies for these PFTs (Huang et al., 2016b; Asaadi et al., 2018). The introduction of lateral soil water flow algorithms does not hinder its modelling capabilities. The modelling of carbon fluxes and dynamic vegetation growth for crops is often difficult as harvesting and planting times are frequently decided by individuals and user judgement on physical indicators, independently of phenological processes. It does not always align with model assumptions (Bonora et al., 2014; Xu et al., 2019). For example, the timing of the peak GEP and NEP values for crops are reflected and dependent in the choice of parameters such as the timing of leaf onset, timing of the harvest, threshold to commence harvest and the length of the harvest. Although there have been previous studies within or near Big Creek catchment on observing energy fluxes of $C_3$ crops (Davies and Allen, 1973; Bailey and Davies, 1980), there has not yet been a site measuring carbon fluxes for $C_3$ crops for an entire year or for the duration of a single growing season. Due to the relative dominance of $C_3$ crops in Big Creek catchment and throughout southern Ontario, it will be important to set up flux observations over such crops in the future for future MESH-CTEM and other model validation studies.

For the grid average values shown in Figure (15), MESH-CTEM was able to simulate realistic spatial patterns of water and carbon fluxes. As expected, the highest ET rates occurred in the southern parts of the catchment where there are more forests. One exceptional case were grids with a strong urban land-use where there were very little carbon flux exchanges but with relatively high rates of evapotranspiration. In this study, we used a relatively finer ($0.02^o$ x $0.02^o$) grid resolution, while previous regional CTEM simulations had been performed at $0.35^o$ x $0.61^o$ (Peng et al., 2014), $2.8^o$ x $2.8^o$ (Lee et al., 2017), $0.5^o$ x $0.5^o$ (Huang et al., 2016b) or $1.0^o$ x $1.0^o$ (Shrestha et al., 2017) grid resolutions. This finer resolution is more consistent with previous MESH studies using resolutions such as $0.167^o$ x $0.167^o$ (Haghnegahdar et al., 2015; Davison et al., 2016) or $0.125^o$ x $0.125^o$ (Yassin et al., 2019) or $0.01^o$ x $0.01^o$ (Mengistu and Spence, 2016). Having finer grid resolutions for carbon flux helps in improving the representation of the temporal and spatial patterns of terrestrial carbon sources or sinks at a more regional scale (Chen et al., 2003). The mapping and modelling of these sinks and sources is becoming increasingly important due to climate change research and the need for accurately estimating anthropogenic impacts on the global carbon cycle (Tans et al., 1990; Baldocchi et

al., 2003; Fernández-Martínez et al., 2019). Having a finer spatial resolution in the model will also help in simulating PFTs growing in climate niches due to large variations in topography in watershed scale studies (Shrestha et al., 2017). However, increasing the model grid resolution has been well documented to cause an increase in the overall uncertainty and it may not closely align with environmental processes occurring at relatively fine scales (Wiens et al., 2009; Davison et al., 2016).

The continuing development of numerical models simulating the interactions between hydrological and biogeochemical processes such as MESH-CTEM, has been deemed as important for improving land surface models and further understanding the behaviour of catchment-scale and regional carbon fluxes. The development of more accurate and precise hydrological models for watershed/catchment-scale applications has also been labelled as important in order to address issues such as flooding or water availability (Todini, 2007; Chen et al., 2017).

Despite its current limitations, MESH-CTEM has provided the ability to spatially simulate land surface and dynamic vegetative processes at a catchment scale. MESH-CTEM offers alternative algorithms such that, several parameters within CLASS which would no longer require estimations or calibrations. With the added and dynamic biophysics from CTEM, there was an improvement in the runoff generation and overall water dynamics, and thus could be of interest in broader MESH applications, such for flood forecasting. For researchers focusing on CTEM, MESH-CTEM offers a mechanism in which to simulate at a relatively finer scale by letting MESH handle the inter-grid hydrological interactions. Additionally, integrating CTEM and MESH into a single functioning model will hopefully help future researchers to simulate and understand the large diversity of ecohydrological processes within several landscapes. MESH-CTEM will also help in closing existing research gaps between the hydrological and ecological sciences. Furthermore, this study does not claim that the improvements shown at the Big Creek catchment are clear indicators that CTEM is guaranteed to improve MESH simulations in other domains. Thus, further testing of MESH-CTEM for multiple catchments across different landscapes is recommended to further investigate the impact of CTEM on traditional hydrological simulations. Additional testing of CTEM's other capabilities such as nitrogen cycling and adding wetlands as a PFT is recommended to further investigate these processes and their effects on catchment-scaled hydrology.

## 5. Conclusion

This study developed an integrated hydrological and biogeochemical modelling system, MESH-CTEM by adding the CLASS-CTEM land-surface model to the MESH modelling system. The model was tested at the Big Creek catchment in southern Ontario over the period October 1$^{st}$ 2004 to December 31$^{st}$ 2017 using observed flux, meteorological and hydrological datasets.

Simulated hydrological processes showed significant improvements due to changes attributed to the parameterization of canopy conductance, soil water regimes and carbon cycle feedbacks. Most importantly, CTEM's indirect impact on streamflow helped to provide a more accurate calibration procedure over the Big Creek catchment.

MESH-CTEM was able to simulate dynamic vegetation growth across all PFTs found with the Big Creek Basin. Modelled GEP, Re and NEP values were comparable with previous studies using CLASS-CTEM in literature and the observations from nearby eddy covariance flux tower sites.

Overall, the development of the integrated MESH-CTEM modelling system will help hydrologists in simulating catchment scale processes more accurately by including more realistic vegetation phenology behaviour in model simulations. Future research using MESH-CTEM will contribute to a greater understanding of catchment scale processes under changing climates and provide the necessary tools to address problems within the realm of watershed hydrology.

## 6. References


Abraha, M., Gelfand, I., Hamilton, S. K., Shao, C., Su, Y. J., Robertson, G. P., and Chen,J. (2016). Ecosystem Water-Use Efficiency of Annual Corn and Perennial Grasslands: Contributions from Land-Use History and Species Composition. *Ecosystems*, 19(6):1001-1012

Alavi, N., Bélair, S., Fortin, V., Zhang, S., Husain, S. Z., Carrera, M. L., and Abrahamowicz, M. (2016). Warm Season Evaluation of Soil Moisture Prediction in the Soil, Vegetation and Snow (SVS) Scheme. *Journal of Hydrometeorology*, 17:2315-2332.

Arnold, J. G., Allen, P. M., and Bernhardt, G. (1993). A comprehensive surface-groundwater flow model. *Journal of Hydrology*, 142(1-4):47-69.

Arnold, J. G. and Fohrer, N. (2005). SWAT2000: Current capabilities and research opportunities in applied watershed modelling. *Hydrological Processes*, 19(3):563-572.

Arora, V. K. (2003). Simulating energy and carbon fluxes over winter wheat using coupled land surface and terrestrial ecosystem models. *Agricultural and Forest Meteorology*, 118(1-2):21–47.

Arora, V. K. and Boer, G. J. (2003). A Representation of Variable Root Distribution in Dynamic Vegetation Models. *Earth Interactions*, 7(5):1–19.

Arora, V. K. and Boer, G. J. (2005). A parameterization of leaf phenology for the terrestrial ecosystem component of climate models. *Global Change Biology*, 11(1):39–59.

Arora, V. K., Boer, G. J., Christian, J. R., Curry, C. L., Denman, K. L., Zahariev, K., Flato,G. M., Scinocca, J. F., Merryfield, W. J., and Lee, W. G. (2009). The Effect of terrestrial photosynthesis down regulation on the twentieth-century carbon budget simulated with the CCCma Earth System Model. *Journal of Climate*, 22(22):6066–6088.

Asaadi, A., Arora, V. K., Melton, J. R., and Bartlett, P. (2018). An improved parameterization of leaf area index (LAI) seasonality in the Canadian Land Surface Scheme (CLASS) and Canadian Terrestrial Ecosystem Model (CTEM) modelling framework. *Biogeosciences*, 15(22):6885–6907.

Bailey, W. G. and Davies, J. A. (1981). Evaporation from soybeans. *Boundary-Layer Meteorology*, 20(4):417-428.

Baldocchi, D. D. (2003). Assessing the eddy covariance technique for evaluating carbon dioxide exchange rates of ecosystems: past, present and future. *Global Change Biology*, 9(4):479-492.

Ball, J. T., Woodrow, I. E., and Berry, J. A. (1987). A Model Predicting Stomatal Conductance and its Contribution to the Control of Photosynthesis under Different Environmental

Conditions. *Progress in Photosynthesis Research*, (953):221-224.

Bartlett, P., MacKay M. D. and Verseghy D. (2006) Modified Snow Algorithms in the Canadian Land Surface Scheme: Model Runs and Sensitivity Analysis at Three Boreal Forest Stands. *Atmosphere-Ocean,* 44(3):207-222.

Beamesderfer E.R, Arain M.A, Khomik M., and Brodeur J.J. (2019). How will the carbon fluxes within the northernmost temperate deciduous forests of North America fair under future climates? *Journal of Geophysical Research - Biogeosciences* (in review).

Bond, B. (2003). Hydrology and ecology meet? And the meeting is good. *Hydrological Processes*, 17(10):2087–2089.

Bonora, E., Noferini, M., Stefanelli, D., and Costa, G. (2014). A new simple modeling approach for the early prediction of harvest date and yield in nectarines. *Scientia Horticulturae,* 172:1-9.

Buckley, T. N. (2017). Modeling Stomatal Conductance. *Plant Physiology*, 174(2):572-582.

Burrough, P. A. and McDonnell, R. A. (1998). Principles of Geographical Information Systems. *Economic Geography*, 75(4):422.

Canadell, J., Jackson, R. B., Ehleringer, J. B., Mooney, H. A., Sala, O. E., and Schulze, E.-D. (1996). Maximum rooting depth of vegetation types at the global scale. *Oecologia*, 108(4):583–595.

Chapman, L. and Putnam, D. (1984). Physiography of southern Ontario. Technical report, Ontario Geological Survey, Special Volume 2, Toronto.

Chen, J. M., Ju, W., Cihlar, J., Price, D., Liu, J., Chen, W., Pan, J., Black, A., and Barr, A. (2003). Spatial distribution of carbon sources and sinks in Canada's forests. Tellus, Series B: *Chemical and Physical Meteorology*, 55(2):662-641.

Chen, J., Brissette, F. P., and Leconte, R. (2011). Uncertainty of downscaling method in quantifying the impact of climate change on hydrology. *Journal of Hydrology*. 401(4):190-202.

Chen, L., Wang, L., Ma, Y., and Liu, P. (2015). Overview of Ecohydrological Models and Systems at the Watershed Scale. *IEEE Systems Journal*, 9(3):1-9.

Chen, Y., Li, J., Wang, H., Qin, J., and Dong, L. (2017). Large-watershed flood forecasting with high-resolution distributed hydrological model. *Hydrology and Earth System Sciences*, 21(2):735–749. Chow, V. T. (1959). Open-channel hydraulics. *McGraw-Hill Book Company*, page 728.

Clark, M. P., Nijssen, B., Lundquist, J. D., Kavetski, D., Rupp, D. E., Woods, R. A., Freer, J. E., Gutmann, E. D., Wood, A. W., Brekke, L. D., Arnold, J. R., Gochis, D. J., and

Rasmussen, R. M. (2015). A unified approach for process-based hydrologic modeling: 1. Modeling concept. *Water Resources Research*, 51(4):2498–2514.

Damour, G., Simonneau, T., Cochard, H., and Urban, L. (2010). An overview of models of stomatal conductance at the leaf level, 33:1419-1438.

Daniel, E. B. (2011). Watershed Modeling and its Applications: A State-of-the-Art Review. *The Open Hydrology Journal*, 5(1):26-50.

Dargahi, B. and Setegn, S. G. (2011). Combined 3D hydrodynamic and watershed modelling of Lake Tana, Ethiopia. *Journal of Hydrology*, 398(1-2):44–64.

Davies, J. A. and Allen, C. D. (1973). Equilibrium, Potential and Actual Evaporation from Cropped Surfaces in Southern Ontario. *Journal of Applied Meteorology*, 10:331-348.

Davison, B., Pietroniro, A., Fortin, V., Leconte, R., Mamo, M., and Yau, M. (2016). What is Missing from the Prescription of Hydrology for Land Surface Schemes? *Journal of Hydrometeorology*, 44(3):2013–2039.

Devia, G. K., Ganasri, B., and Dwarakish, G. (2015). A Review on Hydrological Models.*Aquatic Procedia*, 4:1001-1007.

Dingman, S. L. (2002). *Physical Hydrology*. Waveland Press, Inc., Long Grove, IL.

Dornes, P. F., Tolson, B. A., Davison, B., Pietroniro, A., Pomeroy, J. W., and Marsh, P. (2008). Regionalisation of land surface hydrological model parameters in subarctic and arctic environments. *Physics and Chemistry of the Earth*, 33(17-18):1081–1089.

Dudula, J. and Randhir, T. O. (2016). Modeling the influence of climate change on watershed systems: Adaptation through targeted practices. *Journal of Hydrology*, 541(B):703-713.

Dunne, J. P., John, J. G., Shevliakova, S., Stouffer, R. J., Krasting, J. P., Malyshev, S. L., Milly, P. C., Sentman, L. T., Adcroft, A. J., Cooke, W., Dunne, K. A., Griffies, S. M., Hallberg, R. W., Harrison, M. J., Levy, H., Wittenberg, A. T., Phillips, P. J., and Zadeh, N. (2013). GFDL's ESM2 global coupled climate-carbon earth system models. Part II: Carbon system formulation and baseline simulation characteristics. *Journal of Climate*, 26(7):2247-2267.

Fatichi, S., Vivoni, E. R., Ogden, F. L., Ivanov, V. Y., Mirus, B., Gochis, D., Downer, C. W., Camporese, M., Davison, J. H., Ebel, B., Jones, N., Kim, J., Mascaro, G., Niswonger, R., Restrepo, P., Rigon, R., Shen, C., Sulis, M., and Tarboton, D. (2016). An overview of current applications, challenges, and future trends in distributed process-based models in hydrology, 537:45-60.

Fernández-Martínez, M., Sardans, J., Chevallier, F., Ciais, P., Obersteiner, M., Vicca, S., Canadell, J. G., Bastos, A., Friedlingstein, P., Sitch, S., Piao, S. L., Janssens, I. A., and Peñuelas, J. (2019). Global trends in carbon sinks and their relationships with CO2 and temperature. *Nature Climate*

*Change*, 9:73-79.

Flato, G. M. (2011). Earth system models: An overview. *Wiley Interdisciplinary Reviews: Climate Change*, 2(6):783-800.

Gerosa, G., Mereu, S., Finco, A., and Marzuoli, R. (2012). Stomatal Conductance Modeling to Estimate the Evapotranspiration of Natural and Agricultural Ecosystems. In *Evapotranspiration - Remote Sensing and Modeling.*

Gerten, D., Schaphoff, S., Haberlandt, U., Lucht, W., and Sitch, S. (2004). Terrestrial vegetation and water balance - Hydrological evaluation of a dynamic global vegetation model. *Journal of Hydrology*, 286(1-4):249–270.

Haghnegahdar, A., Razavi, S., Yassin, F., and Wheater, H. (2017). Multicriteria sensitivity analysis as a diagnostic tool for understanding model behaviour and characterizing model uncertainty. *Hydrological Processes*, 31(25):4462–4476.

Haghnegahdar, A., Tolson, B. A., Craig, J. R., and Paya, K. T. (2015). Assessing the performance of a semi-distributed hydrological model under various watershed discretization schemes. *Hydrological Processes*, 29:4018-4031.

Haghnegahdar, A., Tolson, B. A., Davison, B., Seglenieks, F. R., Klyszejko, E., Soulis, E. D., Fortin, V., and Matott, L. S. (2014). Calibrating environment Canada's MESH modelling system over the Great Lakes Basin. *Atmosphere - Ocean*, 52(4):281–293.

Hamada, S., Ohta, T., Hiyama, T., Kuwada, T., Takahashi, A., and Maximov, T. C. (2004). Hydrometeorological behaviour of pine and larch forests in eastern Siberia. *Hydrological Processes*, 18(1):23–39.

Hendry, M. J., Mendoza, C. A., Kirkland, R. A., and Lawrence, J. R. (1999). Quantification of transient CO2 production in a sandy unsaturated zone. *Water Resources Research*, 35(7):2189–2198.

Heppner, C. S., Ran, Q., VanderKwaak, J. E., and Loague, K. (2006). Adding sediment transport to the integrated hydrology model (InHM): Development and testing. *Advances in Water Resources*, 29(6):930–943.

Huang, S., Arain, M. A., Arora, V. K., Yuan, F., Brodeur, J., and Peichl, M. (2011). Analysis of nitrogen controls on carbon and water exchanges in a conifer forest using the CLASS-CTEMN+ model. *Ecological Modelling*, 222(20-22):3743–3760.

Huang, S., Bartlett, P., and Arain, M. (2016a). An analysis of global terrestrial carbon, water and energy dynamics using the carbon-nitrogen coupled CLASS-CTEMN+ model. *Ecological Modelling*, 336:36-56.

Huang, S., Bartlett, P., and Arain, M. A. (2016b). Assessing nitrogen controls on carbon, water

and energy exchanges in major plant functional types across North America using a carbon and nitrogen coupled ecosystem model. *Ecological Modelling*, 323:12–27.

Janauer, G. A. (2000). Ecohydrology: Fusing concepts and scales. *Ecological Engineering*, 16(1):9–16.

Jarvis, P. G. (1976). The Interpretation of the Variations in Leaf Water Potential and Stomatal Conductance Found in Canopies in the Field. *Philosophical Transactions of the Royal Society B: Biological Sciences*, 273:593-610.

Jenson, S. K. and Domingue, J. O. (1988). Extracting topographic structure from digital elevation data for geographic information system analysis. *Photogrammetric Engineering and Remote Sensing*, 54(11):1593–1600.

Jones, N., Wright, S., and Maidment, D. (1990). Watershed delineation with triangle-based terrain models. *Journal of Hydraulic*, 116(10):1232-1251.

Kelliher, F. M., Leuning, R., Raupach, M. R., and Schulze, E. D. (1995). Maximum conductances for evaporation from global vegetation types. *Agricultural and Forest Meteorology*, 73(1-2):1–16.

Kornelsen, K. C., Davison, B., and Coulibaly, P. (2016). Application of SMOS Soil Moisture and Brightness Temperature at High Resolution with a Bias Correction Operator. *IEEE Journal of Selected Topics in Applied Earth Observations and Remote Sensing*, 9(4):1590–1605.

Kouwen, N. (1988). WATFLOOD: a Micro-Computer Based Flood Forecasting System Based on Real-Time Weather Radar. *Canadian Water Resources Journal*, 13(1):62–77.

Kouwen, N., Soulis, E. D., Pietroniro, A., Donald, J., and Harrington, R. (1993). Grouped response units for distributed hydrologic modeling. *Journal of Water Resources Planning and Management*, 119(3):289–305.

Krysanova, V. and Arnold, J. G. (2008). Advances in ecohydrological modelling with SWAT-a review. *Hydrological Sciences Journal*, 53(5):939–947.

Kula, M. (2013). *Determining the effects of climate variability and forest thinning on above ground carbon in temperate forests*. MSc thesis, McMaster University.

Latifovic, R., Pouliot, D., and Olthof, I. (2017). Circa 2010 land cover of Canada: Local optimization methodology and product development. *Remote Sensing*, 9(11): 1098.

Lawrence, D., Oleson, K. W., Flanner, M. G., Thornton, P. E., Swenson, S. C., Lawrence, P. J., Zeng, X., Yang, Z.-L., Levis, S., Sakaguchi, K., Bonan, G. B., and Slater, A. G. (2011). Parameterization Improvements and Functional and Structural Advances in Ver- sion 4 of the Community Land Model. *Journal of Advances in Modeling Earth Systems*, 3:27.

Leavesley, G. H., Lichty, R., Troutman, B., and Saindon, L. (1983). Precipitation-Runoff Modeling System: User's Manual. *USGS, Water Resources Investigations Report 83-4238*, page 207.

Lee, J., McKenney, D. W., Pedlar, J. H., and Altaf Arain, M. (2017). Biophysical and economic analysis of black spruce regeneration in eastern Canada using global climate model productivity outputs. *Forests; 8*(4), 106

Leuning, R., Kelliher, F. M., De Pury, D. G., and Schulze, E. D. (1995). Leaf nitrogen, photosynthesis, conductance and transpiration: scaling from leaves to canopies. *Plant, Cell & Environment*, 18:1183-1200.

Liang, X., Lettenmaier, D. P., Wood, E. F., and Burges, S. J. (1994). A simple hydrologically based model of land surface water and energy fluxes for general circulation models. *Journal of Geophysical Research*, 99(D7):14415.

Long Point Region Conservation Authority (2008). Long Point Region Watershed Characterization Report. Technical report.

MacDonald, M. K., Davison, B. J., Mekonnen, M. A., and Pietroniro, A. (2016). Comparison of land surface scheme simulations with field observations versus atmospheric model output as forcing. *Hydrological Sciences Journal*, 61(16):2860–2871.

Maheu, A., Anctil, F., Gaborit, E., Fortin, V., Nadeau, D. F., and Therrien, R. (2018). A field evaluation of soil moisture modelling with the Soil, Vegetation, and Snow (SVS) land surface model using evapotranspiration observations as forcing data. *Journal of Hydrology*, 558:532–545.

Mahfouf, J.-F., Brasnett, B., and Gagnon, S. (2007). A Canadian Precipitation Analysis (CaPA) Project: Description and Preliminary Results. *Atmosphere-Ocean*, 45(1):1-17.

Mailhot, J., Bélair, S., Lefaivre, L., Bilodeau, B., Desgagné, M., Girard, C., Glazer, A., Leduc, A. M., Méthot, A., Patoine, A., Plante, A., Rahill, A., Robinson, T., Talbot, D., Tremblay, A., Vaillancourt, P., Zadra, A., and Qaddouri, A. (2006). The 15-km version of the Canadian regional forecast system. *Atmosphere – Ocean*, 44(2):133-149.

Martinez-Martinez, E., Nejadhashemi, A. P., Woznicki, S. A., and Love, B. J. (2014). Modeling the hydrological significance of wetland restoration scenarios. *Journal of Environmental Management*, 133:121-134.

McDonnell, J. J., Sivapalan, M., Vaché, K., Dunn, S., Grant, G., Haggerty, R., Hinz, C., Hooper, R., Kirchner, J., Roderick, M. L., Selker, J., and Weiler, M. (2007). Moving beyond heterogeneity and process complexity: A new vision for watershed hydrology. *Hydrological Processes*, 24, 1745–1754

McGinn, S. M. and King, K. M. (1990). Simultaneous measurements of heat, water vapour and CO2 fluxes above alfalfa and maize. *Agricultural and Forest Meteorology*. 49(4):331-349.

McKenzie, S. M., Slater, G., Kim, S.-T., Pisaric, M. F. J., and Arain, M. A. (2018). Influence of seasonal temperature on tree ring $\delta$13C in different-aged temperate pine forests. *Forest Ecology and Management*, 419-420:197–205.

Mekonnen, M. A., Wheater, H. S., Ireson, A. M., Spence, C., Davison, B., and Pietroniro, A. (2014). Towards an improved land surface scheme for prairie landscapes. *Journal of Hydrology*, 511:105–116.

Melton, J. R. and Arora, V. K. (2016). Competition between plant functional types in the Canadian Terrestrial Ecosystem Model (CTEM) v. 2.0. *Geoscientific Model Development*, 9(1):323–361.

Nash, J. E. and Sutcliffe, J. V. (1970). River flow forecasting through conceptual models part I - A discussion of principles. *Journal of Hydrology*, 10(3):282-290.

O'Callaghan, J. F. and Mark, D. M. (1984). The extraction of drainage networks from digital elevation data. *Computer Vision, Graphics, and Image Processing*, 28(3):323-344.

Pan, H. L. and Mahrt, L. (1987). Interaction between soil hydrology and boundary-layer development. *Boundary-Layer Meteorology*, 38(1-2):185-202.

Pattison-Williams, J. K., Pomeroy, J. W., Badiou, P., and Gabor, S. (2018). Wetlands, Flood Control and Ecosystem Services in the Smith Creek Drainage Basin: A Case Study in Saskatchewan, Canada. *Ecological Economics,* 147:36-47.

Peel, M. C., Finlayson, B. L., and McMahon, T. A. (2007). Updated world map of the Köppen-Geiger climate classification, *Hydrology and Earth Systems Sciences*, 11(5): 1633-1644.

Peichl, M. and Arain, M. A. (2006). Above- and belowground ecosystem biomass and carbon pools in an age-sequence of temperate pine plantation forests. *Agricultural and Forest Meteorology*, 140(1-4):51–63.

Peichl, M., Brodeur, J. J., Khomik, M., and Arain, M. A. (2010). Biometric and eddy-covariance based estimates of carbon fluxes in an age-sequence of temperate pine forests. *Agricultural and Forest Meteorology,* 150(7-8):952-965.

Peng, Y., Arora, V. K., Kurz, W. A., Hember, R. A., Hawkins, B. J., Fyfe, J. C., and Werner, A. T. (2014). Climate and atmospheric drivers of historical terrestrial carbon uptake in the province of British Columbia, Canada. *Biogeosciences*.

Pietroniro, A., Fortin, V., Kouwen, N., Neal, C., Turcotte, R., Davison, B., Verseghy, D., Soulis, E. D., Caldwell, R., Evora, N., and Pellerin, P. (2007). Development of the MESH modelling

system for hydrological ensemble forecasting of the Laurentian Great Lakes at the regional scale. *Hydrology and Earth System Sciences*, 11(4):1279–1294.

Pietroniro, A., and Soulis, E. D. (2003). A hydrology modelling framework for the Mackenzie GEWEX programme. *Hydrological Processes,* 17(3): 673-676.

Pohl, S., Davison, B., Marsh, P., and Pietroniro, A. (2005). Modelling spatially distributed snowmelt and meltwater runoff in a small arctic catchment with a hydrology land-surface scheme (watclass). *Atmosphere - Ocean*, 43(3):193–211.

Porporato, A. and Rodriguez-iturbe, I. (2002). Ecohydrology - a challenging multidisciplinary research perspective. *Hydrological Sciences Journal*, 47(5):811–821.

Richards, L. A. (1931). Capillary conduction of liquids through porous mediums. *Journal of Applied Physics*, 1(5):318–333.

Richardson, A. H. (1953). Big Creek Valley conservation report 1953. Technical report, Department of Planning and Development, Toronto.

Rodriguez-Iturbe, I. (2000). Ecohydrology: A hydrologic perspective of climate-soil-vegetation dynamics.

Santhi, C., Srinivasan, R., Arnold, J. G., and Williams, J. R. (2006). A modeling approach to evaluate the impacts of water quality management plans implemented in a watershed in Texas. *Environmental Modelling and Software*.

Shao, P., Zeng, X., Sakaguchi, K., Monson, R. K., and Zeng, X. (2013). Terrestrial carbon cycle: Climate relations in eight CMIP5 earth system models. *Journal of Climate*, 26(22):8744–8764.

Shortt, R., Caldwell, W. J., Ball, J., and Agnew, P. (2009). A Participatory Approachto Water Management: Irrigation Advisory Committees in Southern Ontario. *Canadian Water Resources Journal*, 31(1):13-24.

Shrestha, R. K., Arora, V. K., Melton, J. R., and Sushama, L. (2017). An assessment of geographical distribution of different plant functional types over North America simulated using the CLASS-CTEM modelling framework. *Biogeosciences Discussions*, pages 1–43.

Singh, V. P. and Frevert, D. K. (2002). *Mathematical Models of Large Watershed Hydrology*, Water Resources Publications, 891 pp., Highlands Ranch,Colo.

Sinnathamby, S. (2014) *Modelling tools for ecohydrological characterization.* PhD thesis, Kansas State University.

Snelgrove, K. R. (2002). *Implications of Lateral Flow Generation on Land-Surface Scheme Fluxes*. PhD thesis, University of Waterloo.

Soulis, E. D., Craig, J. R., Fortin, V., and Liu, G. (2011). A simple expression for the bulk field capacity of a sloping soil horizon. *Hydrological Processes*, 25(1):112-116.

Soulis, E. D., Snelgrove, K. R., Kouwen, N., Seglenieks, F., and Verseghy, D. L. (2000). Towards closing the vertical water balance in Canadian atmospheric models: Coupling of the land surface scheme class with the distributed hydrological model watflood. *Atmosphere-Ocean*, 38(1):251-269.

Statistics Canada (2012). 2011 Census Profile. *Census Profile*.

Suyker, A. E. and Verma, S. B. (2009). Evapotranspiration of irrigated and rainfed maize-soybean cropping systems. *Agricultural and Forest Meteorology*, 149(3-4):443-452.

Tague, C. L. and Band, L. E. (2004a). RHESSys: Regional Hydro-Ecologic Simulation System An Object-Oriented Approach to Spatially Distributed Modeling of Carbon, Water, and Nutrient Cycling. *Earth Interactions*, 8(19):1-42.

Tang, Y., Marshall, L., Sharma, A., and Ajami, H. (2018). A Bayesian alternative for multi-objective ecohydrological model specification. *Journal of Hydrology*, 556: 25-38.

Tans, P. P., Fung, I. Y., and Takahashi, T. (1990). Observational constraints on the global atmospheric CO2 budget. *Science*, 247(4949):1431-1438.

Taylor, K. E., Stouffer, R. J., and Meehl, G. A. (2012). An overview of CMIP5 and the experiment design, *American Meteorological Society*, 93:485-498.

Tetzlaff, D., Soulsby, C., Bacon, P. J., Youngson, A. F., Gibbins, C., and Malcolm, I. A. (2007). Connectivity between landscapes and riverscapes—a unifying theme in integrating hydrology and ecology in catchment science? *Hydrological Processes*, 21(10):1385-1389.

Thornton, P. K., Jones, P. G., Alagarswamy, G., and Andresen, J. (2009). Spatial variation of crop yield response to climate change in East Africa. *Global Environmental Change*, 19(1):54-65.

Todini, E. (2007). Hydrological catchment modelling: Past, present and future. *Hydrology and Earth System Sciences*, 11(1):468-482.

Tolson, B. A. and Shoemaker, C. A. (2007). Dynamically dimensioned search algorithm for computationally efficient watershed model calibration. *Water Resources Research*, 43.

Trant, S. J. (2014). *Effects of thinning on carbon dynamics in a temperate coniferous forest*. M.Sc. thesis, McMaster University.

Troendle, C. A. and King, R. M. (1987). The effect of partial and clearcutting on streamflow at Deadhorse Creek, Colorado. *Journal of Hydrology*, 90(1-2):145–157.

Verseghy, D. L. (1991). Canadian Land Surface Scheme for GCMS I. Soil model. *International Journal of Climatology*, 11:111–133.

Verseghy, D. L. (2012). CLASS - The Canadian land surface scheme, Manual/Documentation, version 3.6. Technical report, Climate Research Division, Science and Technology Branch, Environment Canada.

Verseghy, D. L., McFarlane, N. A., and Lazare, M. (1993). Class - A Canadian land sur- face scheme for GCMS, II. Vegetation model and coupled runs. *International Journal of Climatology*, 13(4):347–370.

Wicks, J. M. and Bathurst, J. C. (1996). SHESED: A physically based, distributed erosion and sediment yield component for the SHE hydrological modelling system. *Journal of Hydrology*, 175(1-4):213–238.

Wiens, J. A., Stralberg, D., Jongsomjit, D., Howell, C. A., and Snyder, M. A. (2009). Niches, models, and climate change: assessing the assumptions and uncertainties. Proceedings of the National Academy of Sciences of the United States of America, 106(2):19729 –19736.

Wu, Y., Verseghy, D. L., and Melton, J. R. (2016). Integrating peatlands into the coupled Canadian Land Surface Scheme (CLASS) v3.6 and the Canadian Terrestrial Ecosystem Model (CTEM) v2.0. *Geoscientific Model Development*, 9(8):2639–2663.

Xu, C. Y. and Singh, V. P. (2004). Review on regional water resources assessment models under stationary and changing climate. *Water Resources Management*, 18(6):591-612.

Xu, J., Meng, J., and Quackenbush, L. J. (2019). Use of remote sensing to predict the optimal harvest date of corn. *Field Crops Research*, 236:1-13.

Xu, X., Li, J., Tolson, B. A., Staebler, R. M., Seglenieks, F., Davison, B., Haghnegahdar, A., and Soulis, E. D. (2014). Assimilation of SMOS soil moisture in the MESH model with the ensemble Kalman filter. In *International Geoscience and Remote Sensing Symposium (IGARSS)*, pages 3766–3769.

Yassin, F., Razavi, S., Wheater, H., Sapriza-Azuri, G., Davison, B., and Pietroniro, A. (2017). Enhanced identification of a hydrologic model using streamflow and satellite water storage data: A multicriteria sensitivity analysis and optimization approach. *Hydrological Processes*, 31(19):3320–3333.

Yuan, F., Arain, M. A., Black, T. A., and Morgenstern, K. (2007). Energy and water exchanges modulated by soil-plant nitrogen cycling in a temperate Pacific Northwest conifer forest. *Ecological Modelling*, 201(3-4):331–347.

Zalewski, M. (2002). Ecohydrology - the use of ecological and hydrological processes for sustainable management of water resources. *Hydrological Sciences*, 47(5):825–834.

Zanchi, G., Belyazid, S., Akselsson, C., Yu, L., Bishop, K., Köhler, S., and Grip, H. (2016). A Hydrological Concept including Lateral Water Flow Compatible with the Biogeochemical Model ForSAFE. *Hydrology*, 3(1):11.

Zavitz, E. J. (1961). Fifty years of reforestation in Ontario. Technical report, Ontario Department of Lands and Forests, Toronto.

Zhang, Y., Grant, R. F., Flanagan, L. B., Wang, S., and Verseghy, D. L. (2005). Modelling CO2and energy exchanges in a northern semiarid grassland using the carbon- and nitrogen- coupled Canadian Land Surface Scheme (C-CLASS). *Ecological Modelling*, 181(4):591–614.

Zhou, L. (2003). Comparison of seasonal and spatial variations of albedos from Moderate-Resolution Imaging Spectroradiometer (MODIS) and Common Land Model. *Journal of Geophysical Research*, 108(D15):4488.

Zhou, C., and Wang, K. (2016). Biological and environmental controls on evaporative fractions at AmeriFlux sites. *Journal of Applied Meteorology and Climatology*, 55(1):145-161

Table 1: A breakdown of how each land-use category from Latifovic et al. (2017) was broken into their respective PFTs.

| Land Use Category | CLASS PFT | CTEM PFT | PFT Short Name | Land Cover (%) |
|---|---|---|---|---|
| Temperate Needleleaf | Needleleaf Trees | Needleleaf Evergreen | NDL-EVG | 0.2 |
| Temperate Broadleaf | Broadleaf Trees | Broadleaf Cold Deciduous | BDL-DCD-COLD | 11.6 |
| Mixed Forest[a] | Needleleaf & Broadleaf Trees | Needleleaf Evergreen & Broadleaf Cold Deciduous | NDL-EVG & BDL-DCD-COLD | 6.8 |
| Temperate Shrubland | Grasses | C3 Grasses | C3-GRASS | 0.1 |
| Temperate Grassland | Grasses | C3 Grasses | C3-GRASS | < 0.1 |
| Wetland | Grasses | C3 Grasses | C3-GRASS | 0.1 |
| Cropland | Crops | C3 Crops & C4 Crops [b] | C3-CROP & C4-CROP[b] | 73.8 |
| Barren Lands | Grasses | C3 Grasses | C3-GRASS | 1.0 |
| Urban | Urban | Urban | | 6.0 |

[a] Mixed Forest land-use type have Needleleaf and Broadleaf PFTs are assumed to be half of the mixed forest category.

[b] Crop Class is split up into C3 crops and C4 crops which have 73% and 27% land usage respectively (Long Point Region Conservation Authority, 2008).

Table 2: The initial carbon pool values used in the .CTM file for the active PFTs; all values are at the beginning of the simulated year.

| CTEM PDF | NDL-EVG[a] | BDL-DCD-COLD[b] | C3-CROPS[c] | C4-CROPS | C3-GRASS[d] | Urban |
|---|---|---|---|---|---|---|
| LAI Range ($m^2$ $m^{-2}$) | 7.0-8.0 | 0.5-8.0 | 0.0-4.0 | 0.0 - 6.0 | 3.0-4.0 | N.A. |
| Vegetation Height (m) | 20.2 | 25.7 | 0.5 | 1.2 | 0.1 | 10.0 |
| Visible Albedo[e] | 0.04 | 0.07 | 0.06 | 0.06 | 0.06 | 0.06 |
| Infrared Albedo[e] | 0.20 | 0.24 | 0.24 | 0.06 | 0.18 | 0.22 |
| Maximum Annual Canopy Mass ($kg/m^2$) | 15.0 | 12.0 | 4.0 | 4.0 | 2.0 | N.A. |
| Green Leaf Mass (kg $C/m^2$) | 0.1 | 0.2 | 0.08 | 0.08 | 0.2 | N.A. |
| Brown Leaf Mass (kg $C/m^2$) | 0.0 | 0.0 | 0.0 | 0.0 | 0.0 | N.A. |
| Stem Mass (kg $C/m^2$) | 7.3 | 7.0 | 0.0 | 0.0 | 0.2 | N.A. |
| Root Mass (kg $C/m^2$) | 1.9 | 1.5 | 0.0 | 0.0 | 1.2 | N.A. |
| Litter Mass (kg $C/m^2$) | 0.5 | 0.5 | 0.1[f] | 0.2 | 1.0 | N.A. |
| Soil Carbon Mass (kg $C/m^2$) | 3.7 | 2.5 | 2.5[f] | 2.5 | 2.5 | N.A. |

[a] Peichl and Arain (2006), (Huang et al., 2011)

[b] Kula (2013)

[c] Initialized for both C4 and C3 crops

[d] Initialized for temperate Shrublands land-use

[e] Zhou (2003)

[f] Canadell et al. (1996)

Table 3: List of the non-site specific CLASS parameters, their respective estimated ranges and references for those ranges used for the calibration process.

| Parameter Name (Code Abbreviation) | Range/Value | Calibrated Values (NL & BL, CR & GR) |
|---|---|---|
| Sand in mineral soil volume (SAND)[a] | 80.0 - 97.0 % | 93.6, 94.0 |
| Clay in mineral soil volume (CLAY) [a] | 1.0 - 10.0 % | 4.5, 5.0 |
| Drainage index (DRN) | 0.0 - 1.0 | 0.31, 0.69 |
| Drainage density (DD) | 2.0 – 100.0 $km^{-1}$ | 22.1, 70.4 |
| Coef. of $k_{sat}$ change in the first meter of soil (GRKF) | 0.01 - 1.0 | 0.54, 0.73 |
| Manning's n (MANN) | 0.015 – 0.035 $s\ m^{-1/3}$ | 0.033, 0.018 |
| Saturated surface hydraulic conductivity (KSAT) | 0.0001 - 0.1 $m\ s^{-1}$ | 0.010, 0.012 |
| WATFLOOD channel roughness factor (WFR2) [b] | 0.02 - 2.0 | 1.43 |

[a] First layer sand and clay content was changed by -15% and +5% respectively.

[b] Only a single river class was chosen

Table 4: Tabular summary of the modelled and simulated streamflow.

| Simulation | Number of Soil Layers | Total Annual Flow ($km^3$) | NSE | RMSE ($km^3$) |
|---|---|---|---|---|
| Observed | - | 0.2334 | - | - |
| MESH | 3 | 0.0966 | -0.14 | 6.21 |
| MESH-CTEM | 3 | 0.1661 | 0.43 | 4.39 |
| MESH | 6 | 0.114 | 0.10 | 5.51 |
| MESH-CTEM | 6 | 0.1621 | 0.38 | 4.39 |

Table 5: Tabular summary of the overall changes in the soil water regime for every PFT and the 4 major lateral soil water components from the 6 layer simulation. $q_{Int}$ and $q_{Base}$ values shown are in $m^3\ m^{-2}\ year^{-1}$ and averaged out for the entire soil profile. QFC values are written separately for each soil layer.

| Flow Component | NL | BL | CR | GR |
|---|---|---|---|---|
| MESH $q_{Int}$ | 0.09 | 0.05 | 0.27 | 0.20 |
| MESH-CTEM $q_{Int}$ | 0.08 | 0.09 | 0.29 | 0.26 |
| MESH $q_{Base}$ | 0.05 | 0.10 | 0.15 | 0.12 |
| MESH-CTEM $q_{Base}$ | 0.26 | 0.29 | 0.29 | 0.22 |
| MESH $QFC_1$ | 0.11 | 0.10 | 0.09 | 0.14 |
| MESH-CTEM $QFC_1$ | 0.10 | 0.10 | 0.05 | 0.06 |
| MESH $QFC_2$ | 0.15 | 0.14 | 0.11 | 0.18 |
| MESH-CTEM $QFC_2$ | 0.13 | 0.11 | 0.02 | 0.08 |
| MESH $QFC_3$ | 0.05 | 0.06 | 0.03 | 0.05 |
| MESH-CTEM $QFC_3$ | 0.05 | 0.04 | 0.00 | 0.02 |
| MESH $QFC_4$ | 0.04 | 0.03 | 0.02 | 0.00 |
| MESH-CTEM $QFC_4$ | 0.02 | 0.02 | 0.00 | 0.00 |
| MESH $QFC_5$ | 0.03 | 0.03 | 0.03 | 0.00 |
| MESH-CTEM $QFC_5$ | 0.02 | 0.02 | 0.00 | 0.00 |
| MESH $QFC_6$ | 0.13 | 0.14 | 0.00 | 0.00 |
| MESH-CTEM $QFC_6$ | 0.08 | 0.10 | 0.00 | 0.00 |

Table 6: Tabular summary of monthly averaged evaporation fluxes from MESH and MESH-CTEM in a sample NDL-EVG PFT compared to TP39.

| Month | Observed ET (mm month$^{-1}$) | MESH ET (mm month$^{-1}$) | MESH-CTEM ET (mm month$^{-1}$) | MESH RMSE (mm day$^{-1}$) | MESH-CTEM RMSE (mm day$^{-1}$) |
|---|---|---|---|---|---|
| January | 6.9 | 19.5 | 21.3 | 0.762 | 0.755 |
| February | 7.5 | 23.7 | 25.4 | 0.797 | 0.774 |
| March | 11.1 | 36.5 | 27.5 | 1.17 | 0.93 |
| April | 26.2 | 78.3 | 51.8 | 1.76 | 1.10 |
| May | 54.9 | 111.0 | 79.1 | 1.97 | 1.14 |
| June | 76.3 | 122.4 | 88.7 | 1.85 | 1.14 |
| July | 80.2 | 118.4 | 84.7 | 1.69 | 1.15 |
| August | 73.7 | 101.0 | 76.1 | 1.26 | 0.97 |
| September | 53.4 | 78.7 | 60.9 | 1.08 | 0.85 |
| October | 34.7 | 58.3 | 46.5 | 0.88 | 0.80 |
| November | 14.9 | 32.6 | 26.2 | 0.76 | 0.69 |
| December | 9.0 | 24.6 | 25.1 | 0.92 | 0.94 |
| Total | 468.0 | 804.1 | 597.5 | 1.34 | 0.99 |

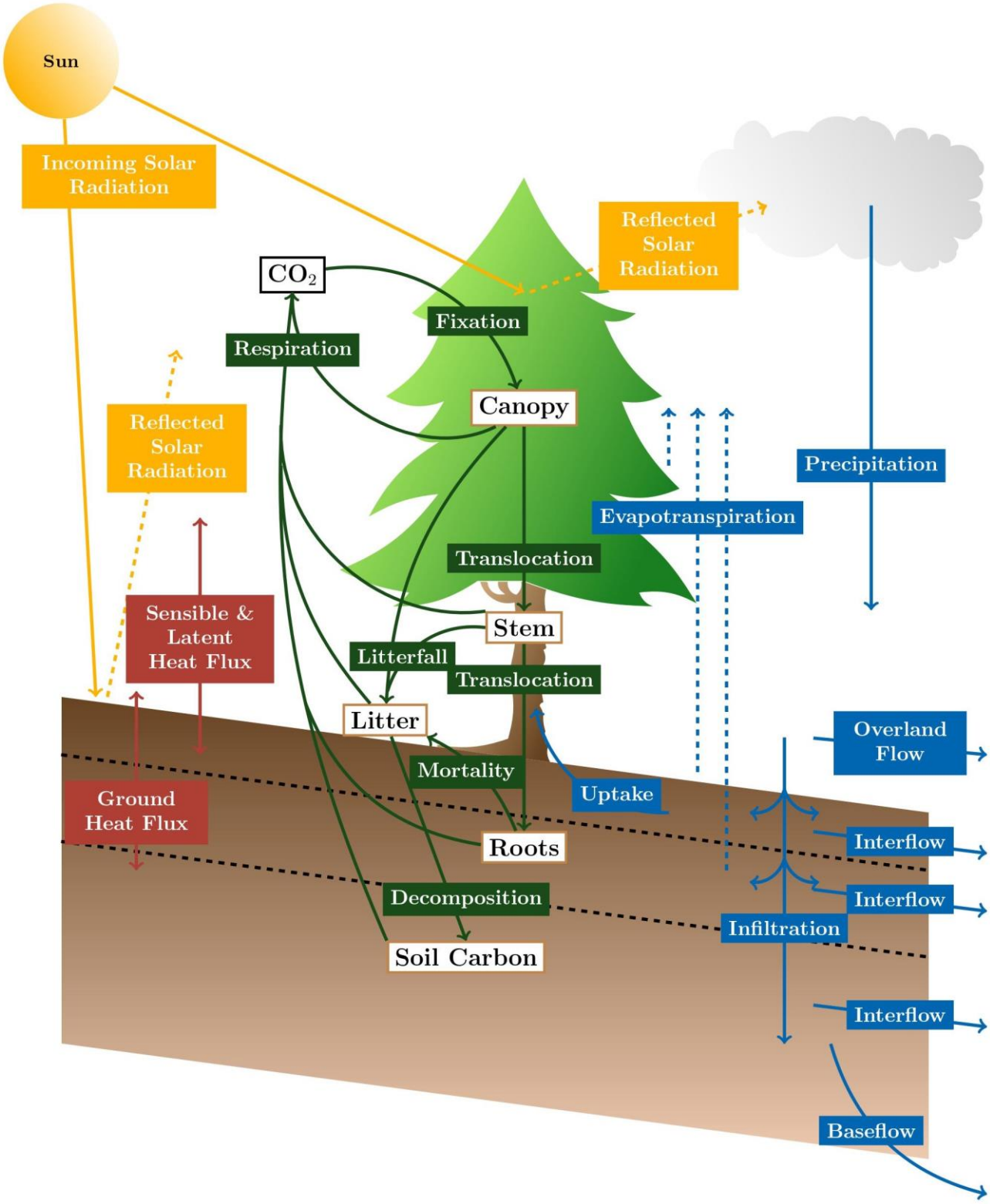


Figure 1: Diagram of the key processes and pools for a GRU within the CLASS-CTEM land model for MESH-CTEM.

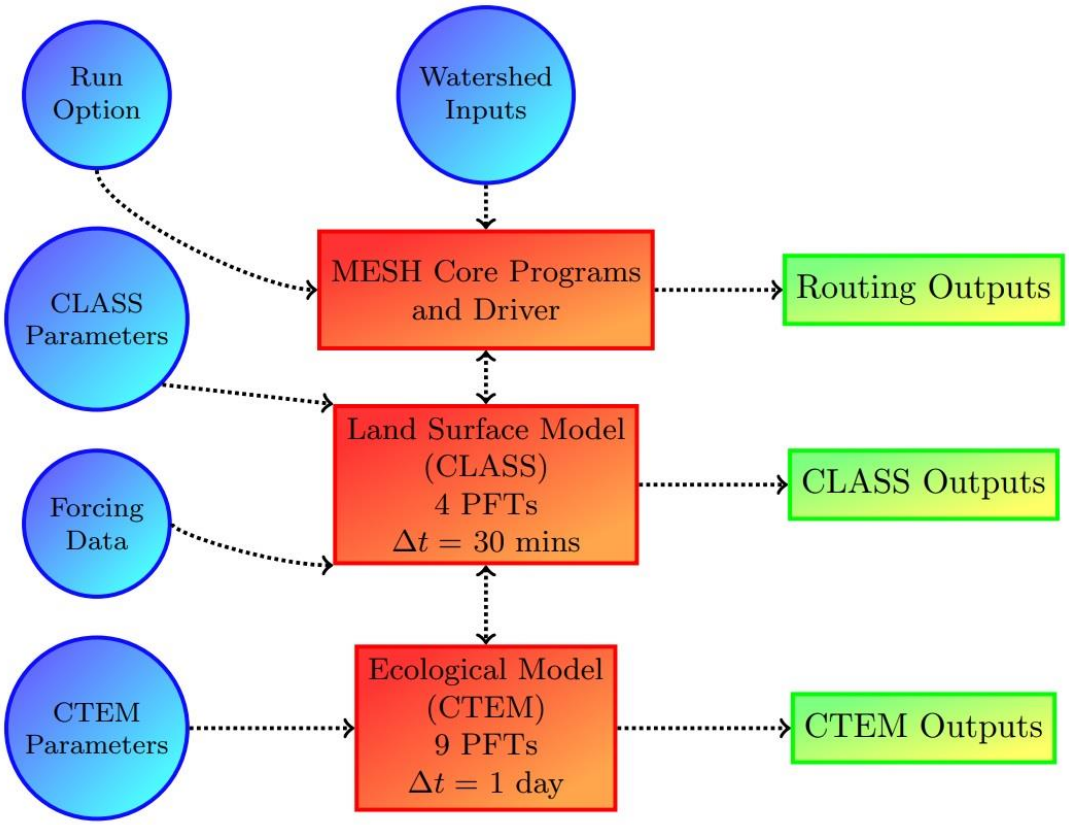


Figure 2: A generalized visual structure of MESH-CTEM with its inputs and outputs.

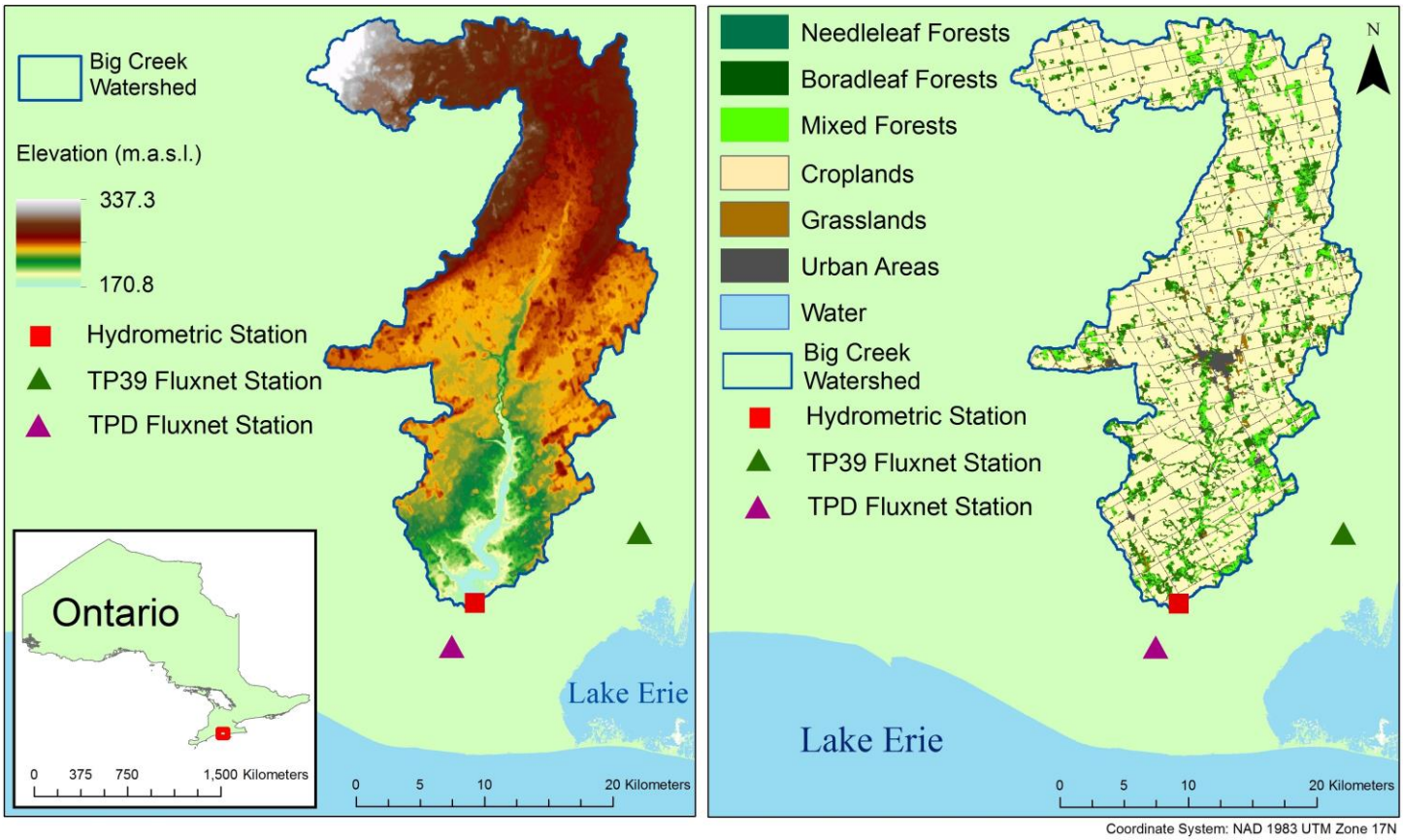


Figure 3: Location of the Big Creek catchment within the province of Ontario including the Walsingham Hydrometric Station and two FluxNet stations.

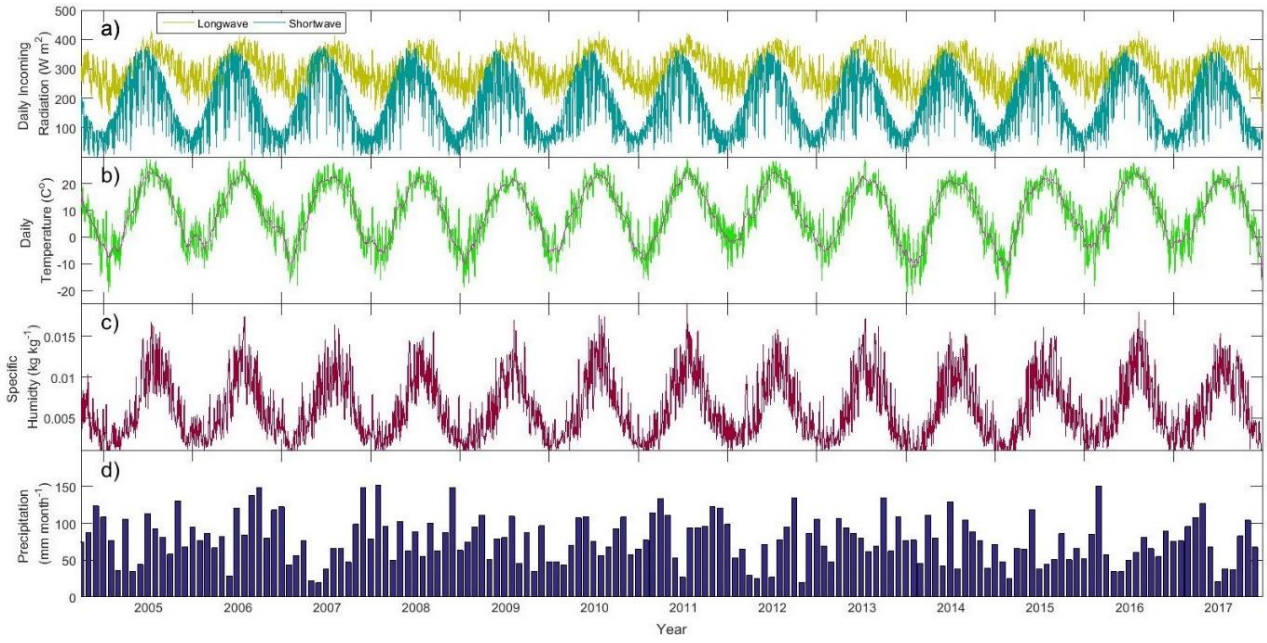


Figure 4: Forcing data summary over the modelled Big Creek area, (a) daily observed longwave and shortwave radiation, (b) daily temperature (in green) with a monthly average temperature (in red), (c) daily average specific humidity and (d) monthly accumulated precipitation.

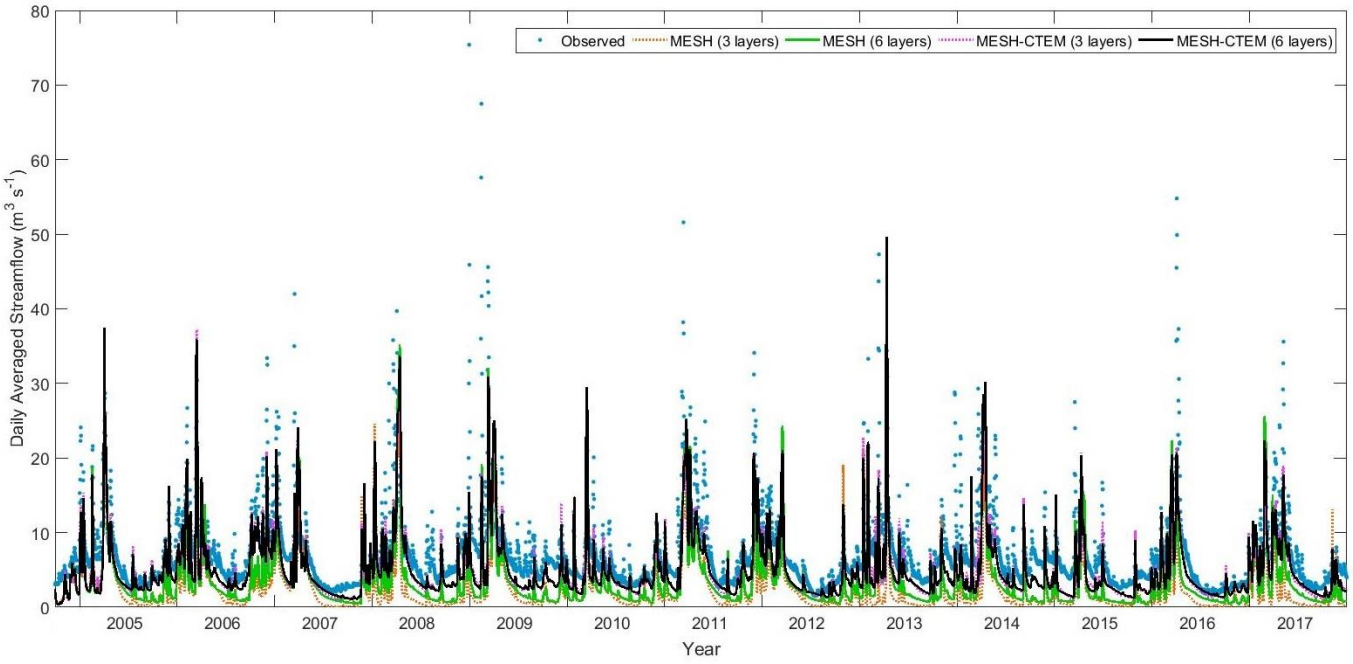


Figure 5: Comparison of the observed and simulated daily streamflow values at the Walsingham Hydrometric Station.

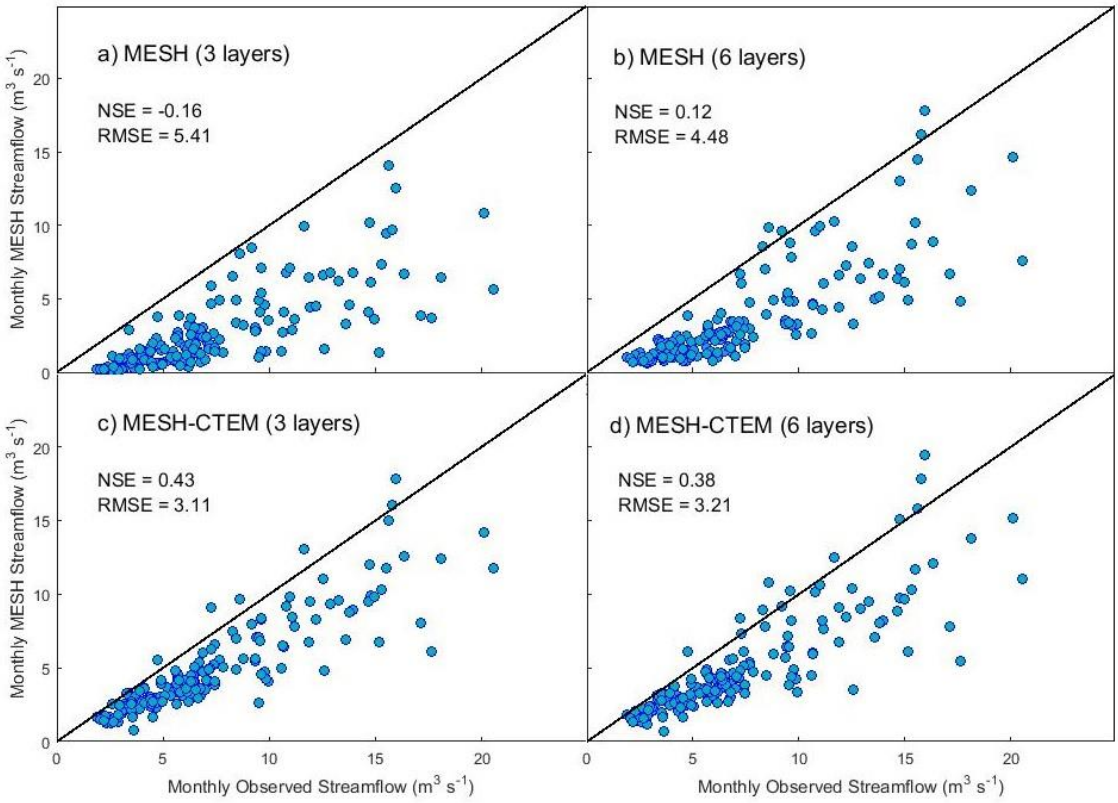


Figure 6: Comparison for simulated monthly averaged streamflow versus observations at Walsingham from the 3- and 6-soil layer model formulations.

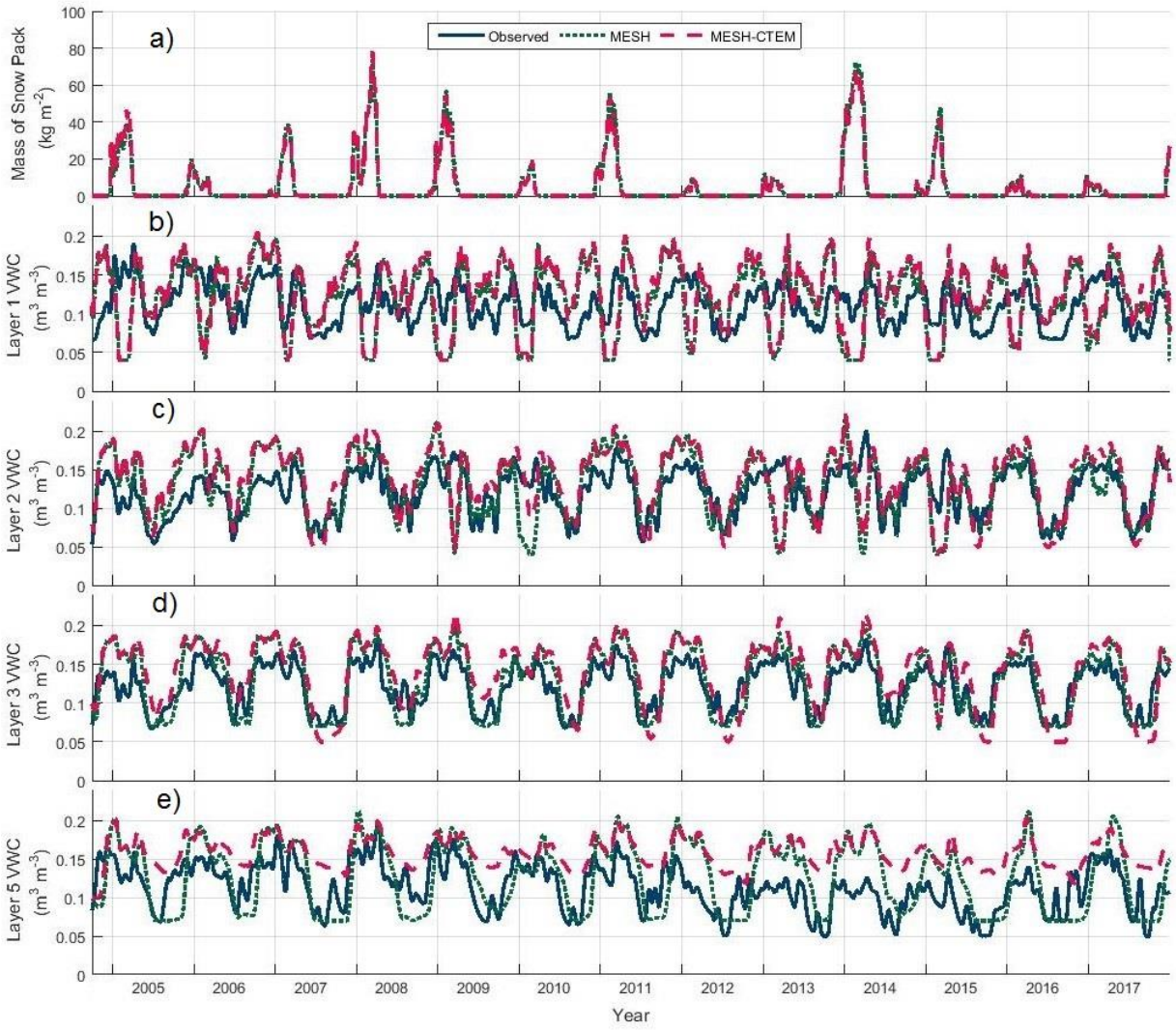


Figure 7: Modelled snow pack mass (a) and monthly mean Volumetric Water Content (VWC) for (b) 5cm (c) 20 cm, (d) 50 cm and (e) 100 cm soil layers for MESH and MESH-CTEM simulations versus observed values at TP39 forest site.

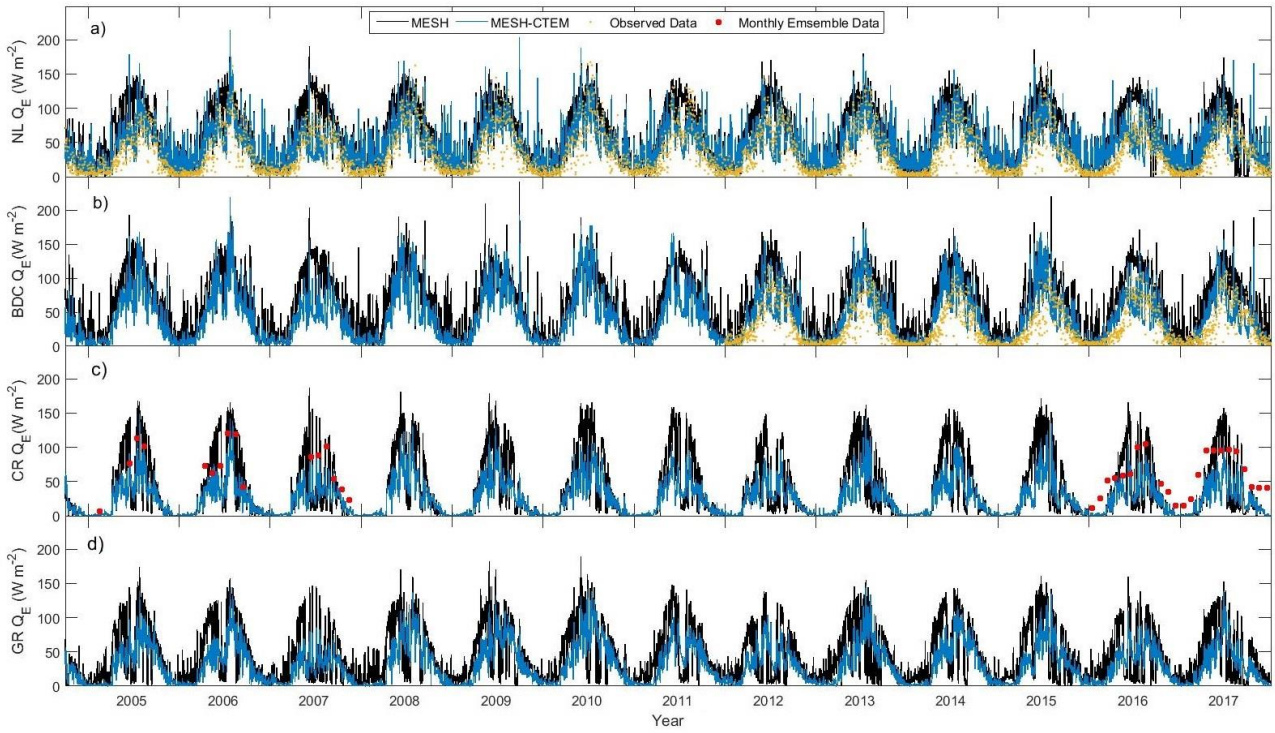


Figure 8: Comparison of latent heat fluxes ($Q_E$) from all four PFTs for MESH and MESH-CTEM. From top to bottom, the simulations are for (a) evergreen needleleaf forests (NL), (b) deciduous broadleaf-cold forests (BDC), (c) crops (CR) and (d) grasses (GR). Observed values for NL, BDC and CR are from TP39, TPD and Elora observations sites.

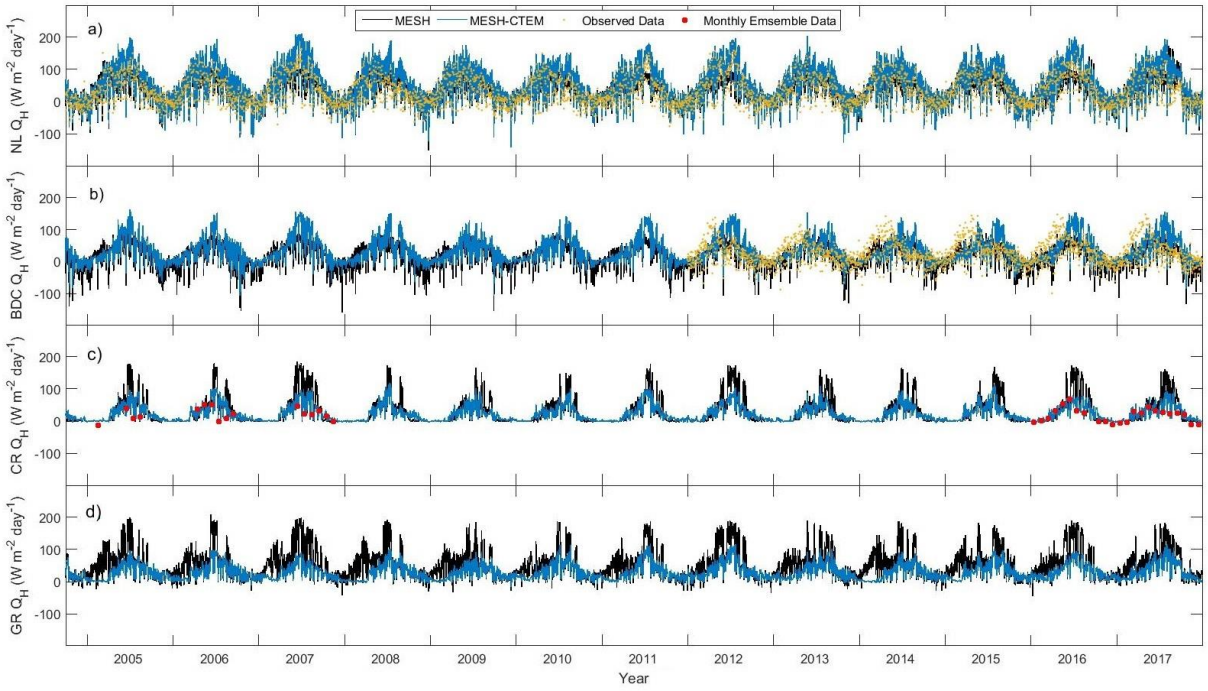


Figure 9: Comparison of Sensible Heat Fluxes ($Q_H$) from all four PFTs for MESH and MESH-CTEM. From top to bottom, the simulations are for (a) evergreen needleleaf forests (NL), (b) deciduous broadleaf-cold forests (BDC), (c) crops (CR) and (d) grasses (GR). Observed values for NL, BDC and CR are from TP39, TPD and Elora observations sites.

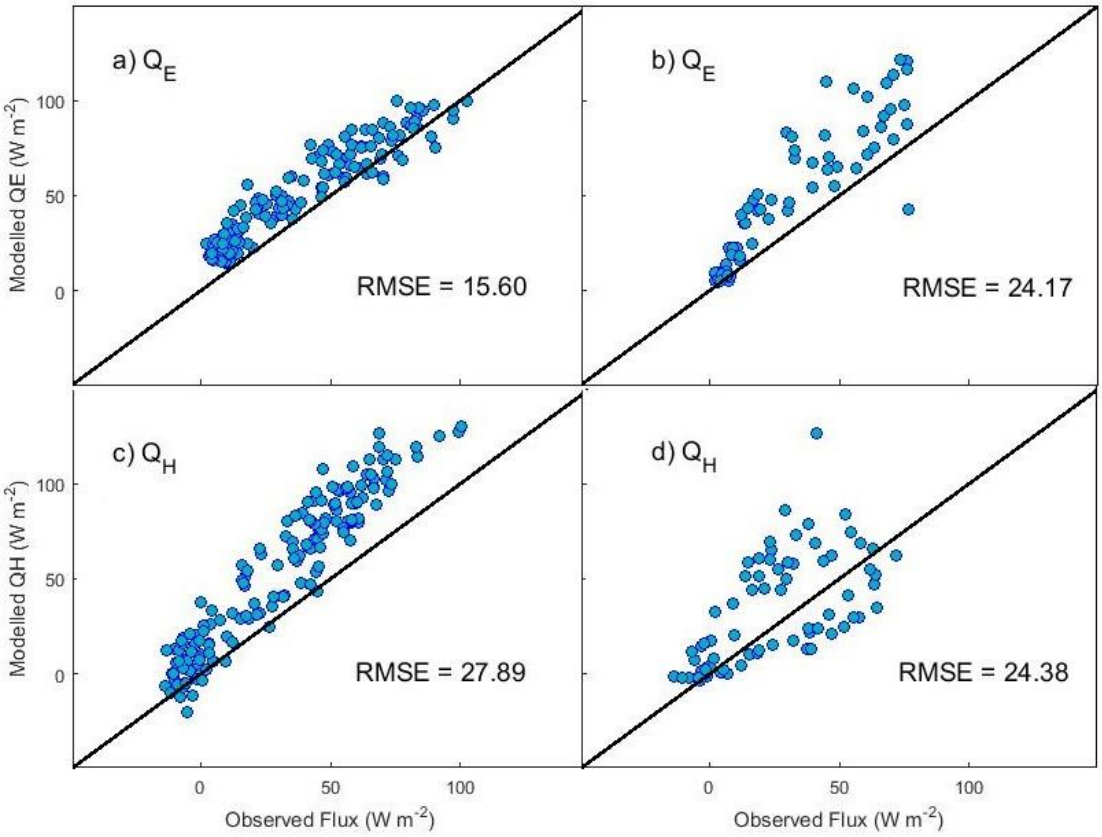


Figure 10: Monthly mean values of simulated latent heat ($Q_E$) and sensible heat ($Q_H$) fluxes (W m$^{-2}$) at EVG-NDL (a, c) and BDL-DCD-COLD (b, d) compared to observations at TPD and TP39 forest sites respectively.

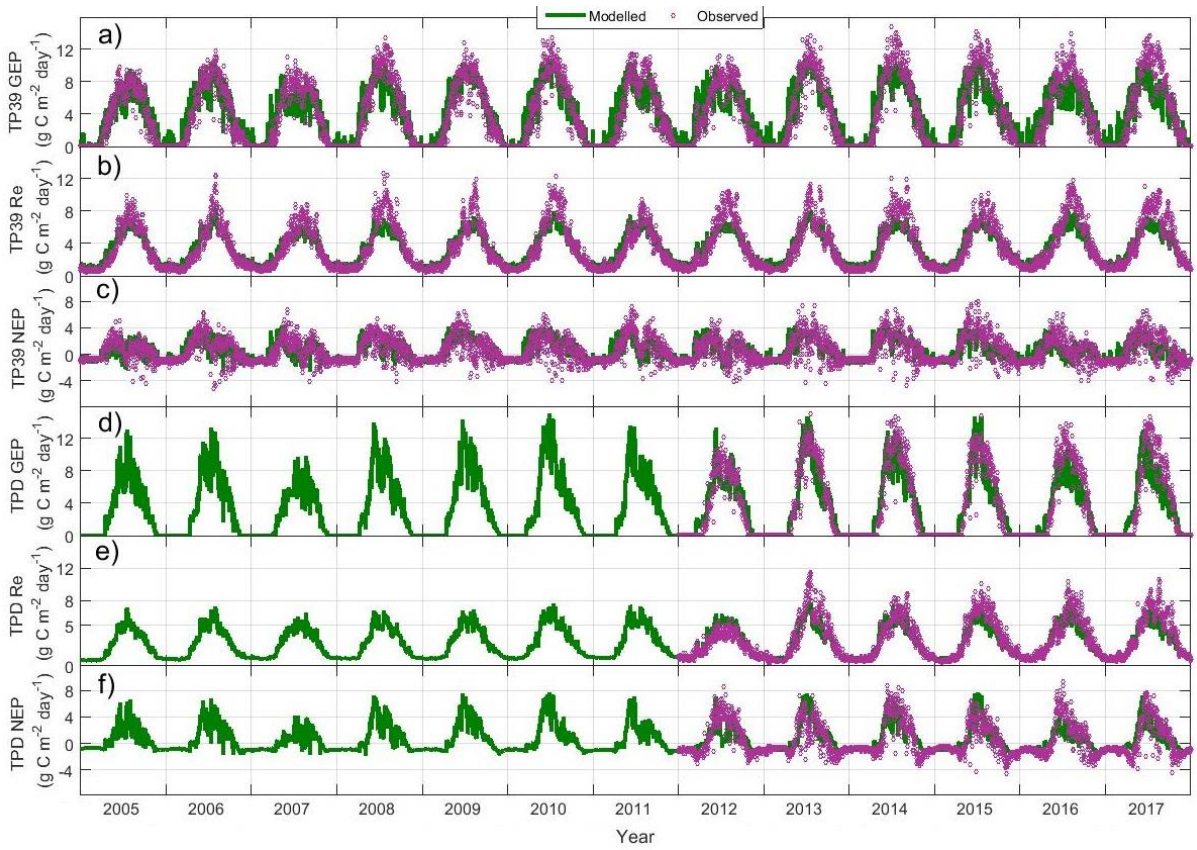


Figure 11: Daily mean values of (a, d) Gross Ecosystem Productivity (GEP), (b, e) Ecosystem Respiration (Re) and (c, f) Net Ecosystem Productivity (NEP) in g C $m^{-2}$ $day^{-1}$ for the EVG-NDL and BDL-DCD-COLD compared to observations at TPD and TP39 forest sites respectively. Observed values are shown as purple dots, while simulations are shown as green lines.

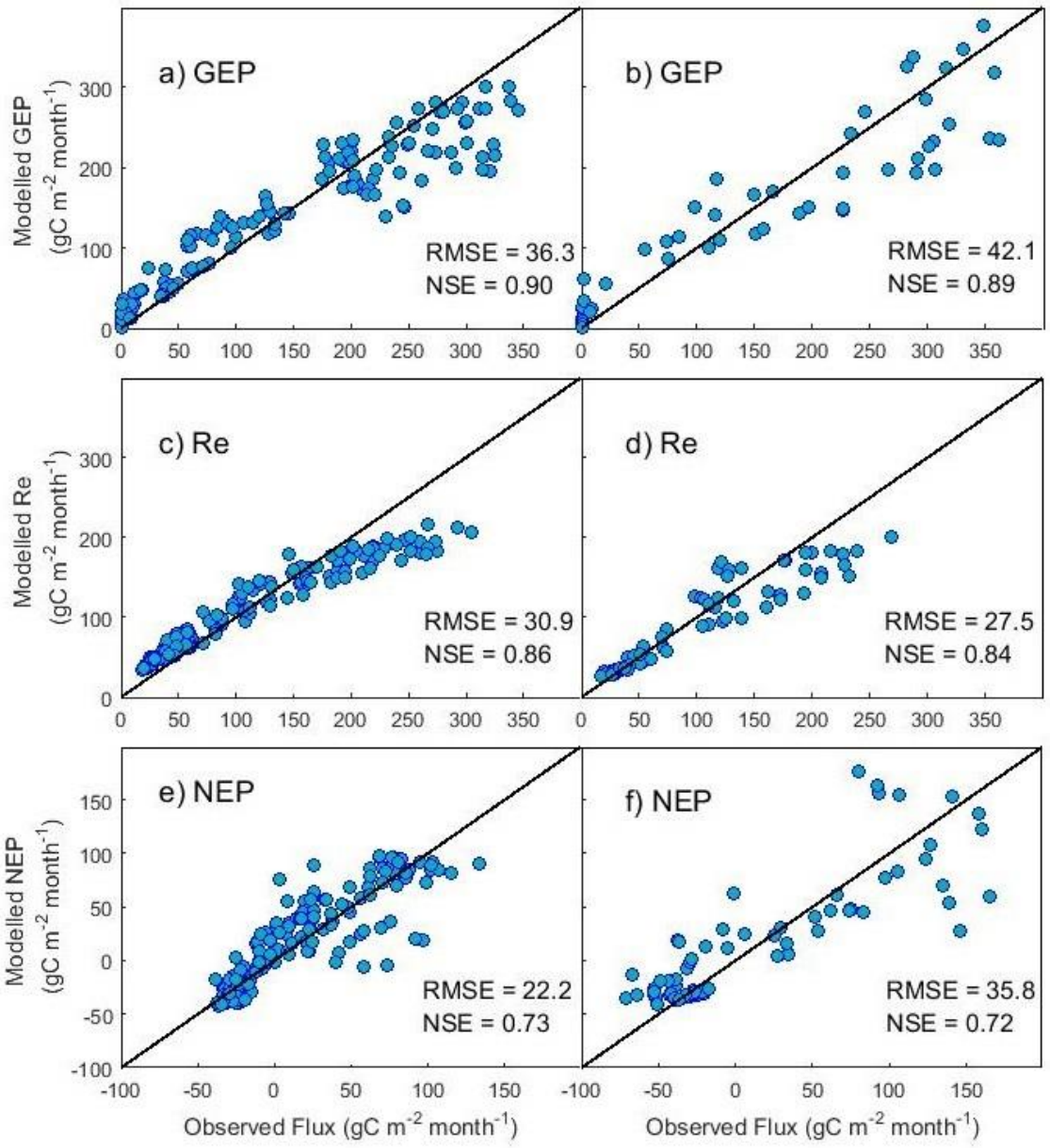


Figure 12. Comparison of monthly mean values of simulated and observed gross ecosystem productivity (GEP), ecosystem respiration (Re) and net ecosystem productivity (NEP) in *g* C $m^{-2}$ $month^{-1}$ for the EVG-NDL (a, c, e) and BDL-DCD-COLD PFT (b, d, f) compared to observations at TPD and TP39 forest sites respectively.

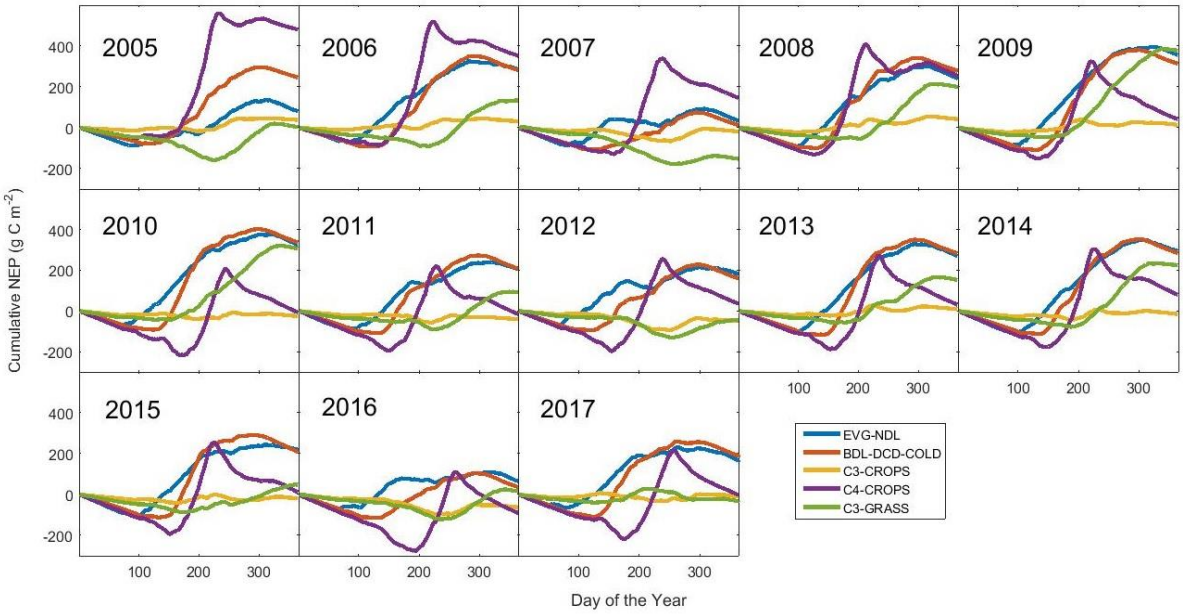


Figure 13 Cumulative Net Ecosystem Productivity (NEP) for each year and each PFT within a single GRU in the Big Creek basin.

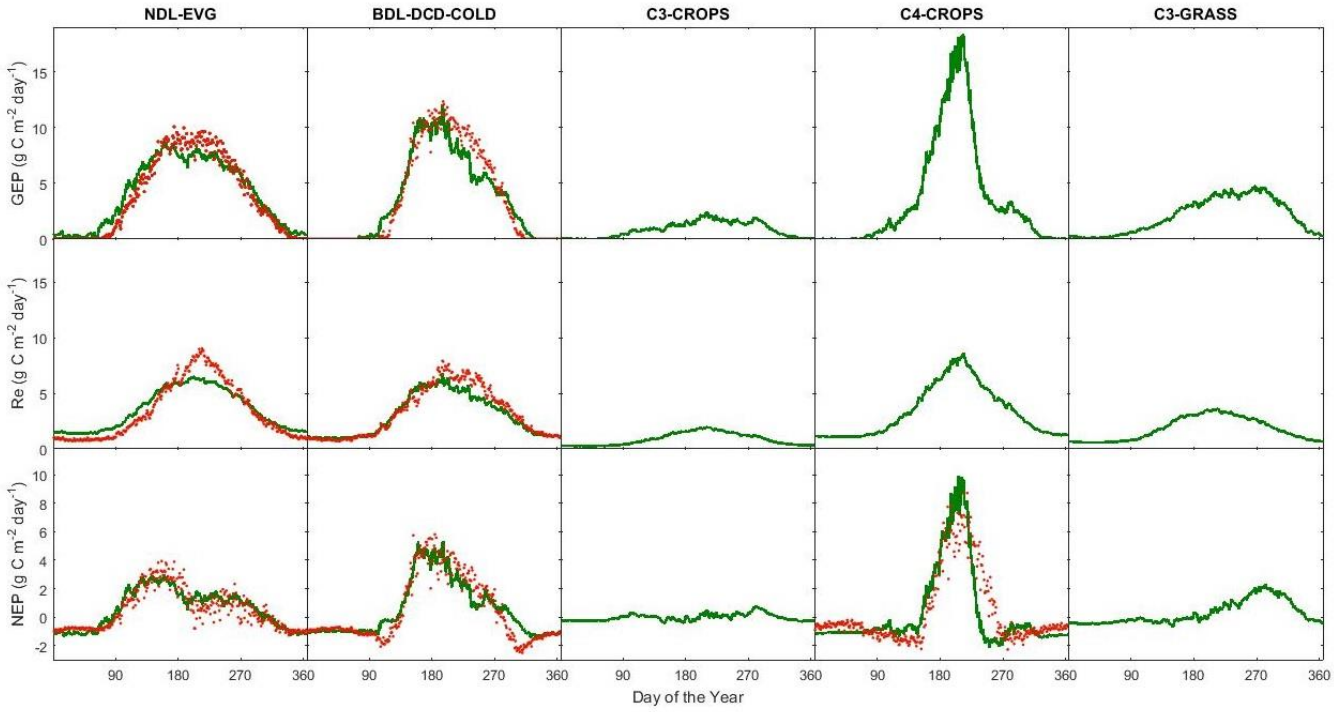


Figure 14: Ensemble gross ecosystem productivity (GEP), ecosystem respiration (Re) and net ecosystem productivity (NEP) in *g* C $m^{-2}$ $day^{-1}$ for all major PFT (Green lines) with available observed data (Red dots) from needleleaf forest, TP39 (2005-2012), deciduous forest, TPD (2012 - 2017) and C4 crop, US-IB1 (2005 - 2016).

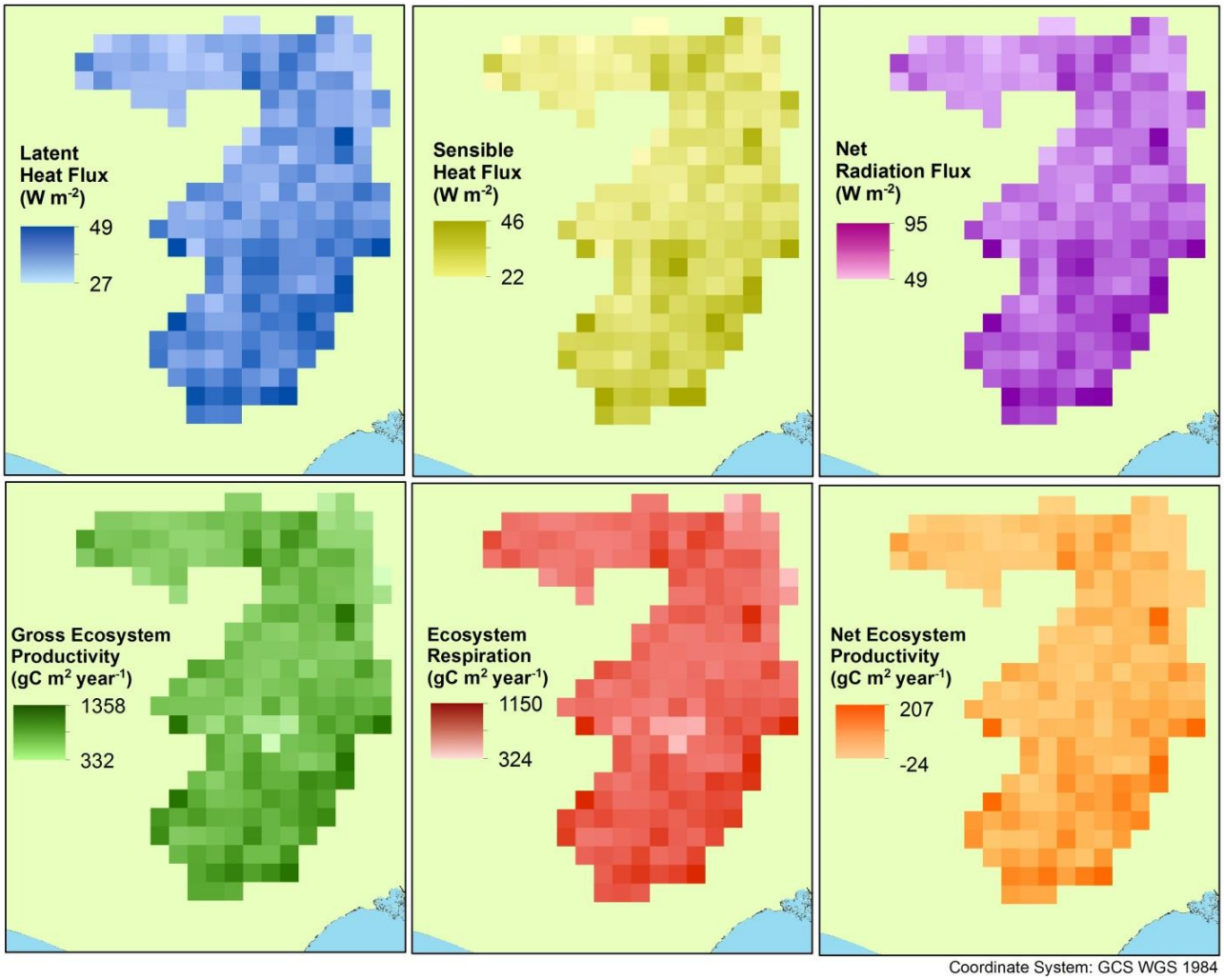


Figure 15: Rasterized output of the MESH-CTEM model within the Big Creek catchment for annual values of energy and carbon fluxes.